MEMORANDUM
RM-3727
NOVEMBER 1965

NUCLEAR EXPLOSIONS IN CAVITIES

H. L. Brode

The RAND Corporation
SANTA MONICA • CALIFORNIA

MEMORANDUM

RM-3727

NOVEMBER 1965

NUCLEAR EXPLOSIONS IN CAVITIES

H. L. Brode

The RAND Corporation
1700 MAIN ST · SANTA MONICA · CALIFORNIA · 90406

PREFACE

The use of underground cavities to muffle or seismically decouple nuclear explosions has been the subject of considerable theoretical effort at RAND. Previous work has suggested that the use of such decoupling can reduce the transmission of seismic signals from underground nuclear detonations by factors of several hundred, depending on such factors as the nature of the cavity wall pressures thus generated. This memorandum reports on the wall pressures and temperatures derived from theoretical calculations of the radiation and hydrodynamic actions from 1.7 KT explosions in 20 and 40 meter cavities filled with air at various densities.

The calculations were made in support of the testimony of A.L. Latter at the Geneva Nuclear Test Ban Conference, December 1959, and the theory developed by Latter, LeLevier, Martinelli, and McMillan as reported in 1961.

Interest in decoupling calculations lagged somewhat during the active nuclear testing period (1961-1963) that followed the three year moratorium (1958-1961). The signing of the partial test ban treaty and the further attempts to extend coverage to a total test ban have provided renewed interest in technical details of cavity explosions such as provided by these numerical results. In addition, the results have found increasing application to possibilities for underground testing where large cavities might be used to explore close-in fireball effects and high temperature, high pressure physics. Recently, several organizations engaged in theoretical planning for future underground tests have expressed interest in these calculations. It is hoped that this Memorandum will be directly applicable to these activities.

SUMMARY

Underground cavities have been suggested as an effective means of reducing the seismic signals from nuclear detonations. This memorandum reports the wall pressures, temperatures, and densities for five specific examples, for which average cavity pressures range between 44 and 420 bars, with peak pressures between 0.2 and 8.2 Kbars. One nuclear yield, 1.7 kilotons, was exploded (theoretically) in two cavities of 20 and 40 meters radius, each with normal and one-tenth normal air density in it. The larger cavity was also used with a density of one-hundredth normal. In addition to the wall pressures, temperatures, and densities as functions of time for each case, some typical pressure, temperature, and density profiles in the cavity interiors at various times are reported.

CONTENTS

I. INTRODUCTION

Following the early theoretical work on seismic decoupling of underground nuclear explosions,[1-4] experimental efforts largely confirmed the suggested range of decoupling factors.[5-7] Such information, combined with the data on transmission of seismic signals from explosive sources,[8-9] has been quite germane to the questions of inspection and enforceability of a more complete test ban treaty and the detection of clandestine tests. The theoretical calculations reported on in this memorandum were undertaken in 1958 as a part of further investigation of the decoupling phenomena suggested and reported in Ref. 1. These calculations define more exactly the pressures and temperatures to which a cavity wall might be exposed for one yield (1.7 KT), two cavity radii (20 and 40 m), and three different air densities (normal, one-tenth normal and one hundredth normal).*

The physical assumptions and limitations which have governed these numerical calculations are briefly outlined and justified in Section II, along with numerical procedures and the mathematical model. The graphical results are presented in Section III together with some interpretive remarks.

---

*The 20 m/one-hundredth normal density calculation was not completed and is not reported because the very small amount of air in that sphere did not significantly alter the wall pressures from those expected in a wholly evacuated sphere.

II. PHYSICAL AND MATHEMATICAL MODEL

The basic physical assumptions of spherical symmetry, thermodynamic equilibrium, radiation diffusion, and hydrodynamics have been shown to be quite valid for the early phases of a nuclear explosion in the atmosphere.[10,11] At late times, when gravity has had time to distort the flow or at times when the motions have slowed considerably allowing instabilities to grow, the spherical symmetry may not be maintained. The problems of interest here are not subject to such distortions until well after the shock reaches the cavity walls, but the late time reverberations reported in Section IV are likely unrealistic to the extent that instabilities and turbulence have destroyed some of the symmetry. Gravity, however, could not have contributed much in times less than a second.

A further assumption which requires some examination is that of no wall response. The walls are here taken to be rigid reflecting surfaces and with very high opacity, so that no shock energy and no radiation flows into them. If the walls are hit hard enough they must move and become heated (and even at low shock inputs the walls will transmit some elastic strain energy), so that whether the walls respond or not is not the question, but rather whether the response has any significant influence on the phenomena inside the cavity. To influence the hydrodynamics appreciably, the walls would have to move in such a way that the shape or volume of the cavity was changed by a few per cent. The consequences of lesser changes in radius or shape would be difficult to distinguish in the results of such a finite difference numerical solution. In a rock cavity large enough that the walls remain elastic in responding to contained explosion, the wall motions are negligible.

Even while the gross response of the walls may be elastic and involve only small strains, there remains some question of the influence of cracks, spalls, rock falls, and wall melt or vaporization. Spalling seems least likely to occur early enough to affect the first reflected pulse or two. Except for rather complicated geological features in the cavity vicinity and for odd shaped cavities or abnormal

shock loads, mechanisms for spall generation do not seem to be present.

Cracks may propagate into the rock and, on opening up under the stress in the cavity, accept an appreciable flow and volume of cavity gas. In such an event, the first pulse reflection is not likely to be influenced, but subsequent cavity pressures and temperatures could be greatly reduced.

To open up an appreciable volume of crack space would, however, require that cavity pressures at relatively late times remain appreciably higher than either the strength (in tension or shear) of the rock or the overburden pressure. Cracks will not form if the walls remain elastic and, even if the walls flow plastically, cracks cannot open until the hoop stress exceeds the compressive stress of the expanding explosive waves. Hoop stresses are developed only as the walls expand radially and can propagate cracks only in regions where radial motions have been sufficient to raise those hoop stresses above the compressive stress plus that of the overburden pressure.

Cavity collapse due to rock falls and chimney formation is always a slow process compared to the shock propagation and reflection times, and no account seems necessary of the effect of such phenomena on the cavity wall pressures and temperatures within the first second.

Wall melt and vaporization could cause the most serious deviation of the cavity phenomena from that predicted on the basis of no wall interaction. Vaporizing even a rather thin layer of wall material can alter appreciably the amount, temperature, or pressure of the cavity gas. It can also appreciably alter the opacities and so the radiative energy transfer properties of the cavity vapors. As suggested in Ref. 1, pressure due to vaporization at the wall is entirely negligible below one electron volt, and may not be serious at even 12 ev. In these examples, wall temperatures fall within or below this range. Fragmentary evidence such as that from the Cowboy Program experiments shows good agreement between calculations and data [12] and indicates that wall interactions do not seriously affect the cavity phenomena for the first several reverberations. The Cowboy comparisons[12] were generally at lower peak pressures and from high explosive sources, however.

With the exception of the rigid boundary which represented the cavity wall and the omission of the thermal radiation loss considerations, these calculations used the same numerical procedures and the same machine program employed for several free air nuclear burst problems. The model is best described in Ref. 10, in which the expression of the hydrodynamic and radiation diffusion mechanisms as differential equations in Lagrangian form are expressed in finite difference form, and procedures for step-wise integration are outlined.

Equations of state and opacities were considered in some detail not only for the air in the cavities but for the various bomb vapors as well. The equation of state for air was included in an analytic form which approximated the theoretical thermodynamic data to within 10% at almost all temperatures and densities.

The weapon was assumed to be composed of spherical shells of appropriate vapors in the interior of which the 1.7 KT of energy was suddenly released. Since, even in the lowest density cases, the bomb vapors do not expand to much more than one half the cavity radius, it is the air rather than the bomb material which is of most concern in describing cavity wall loads. However, mixing and jetting can eventually bring the hot bomb vapors in contact with the walls, where the condensable matter would in the end be deposited.

III. RESULTS

Five separate problems are reported, all for the 1.7 KT weapon in either 20 meter or 40 meter radius cavities. Air densities of normal (ρ_o = 1.293 gm/liter) and one-tenth and one-hundredth normal were used. The following table summarizes some of the parameters observed at the walls for the various cases.

Peak pressures on the wall do not follow a simple scheme. Although doubling the radius drops the wall pressure by eleven-fold at normal air density, it drops by only a little more than a factor of three for the one-tenth normal density case. For a fixed cavity size, the decrease of ambient density and pressure does not guarantee a drop in peak pressure. The average pressure on the wall shows hardly any dependence on the ambient initial density.

The first figure indicates the regularity with which the reverberations progress in the normal density 20 meter cavity case. Wall pressure as a function of time is shown in Fig. 2. At the time labeled "doubled zones," the running time of the numerical problem was increased by coarsening the mass zone system by a factor of two. Such a sudden change in the mass sizes introduces some disturbance, and the subsequent history shows some loss in detail. Wall temperatures for this case are shown in Fig. 3, and air density at the wall is included in Fig. 4. Pressure, temperature, and density all show the same time history details, and the wall conditions are clearly dominated in this case by shocks and hydrodynamic motions.

Pressure profiles for this first case are shown for times before the first reflection in Fig. 5. The shock formation occurs at around 6 meters, and is more clearly illustrated in a subsequent figure (Fig. 12). The complications that arise from secondary shocks is evident in this figure - Fig. 5. A case shock representing the energy of the bomb debris overtakes the main shock just as it reaches the wall and further complicates the reflection there. The reflection factor of around twelve is to be expected at that incident pressure (700 bars).

After reflection the interior zones are so expanded that the shock no longer has a sharp front in a radial profile plot (Fig. 6),

Table

WALL EFFECTS SUMMARY

Air Density (ρ_o)	Cavity Radius (m)	Peak Pressure (kb)	Time at Maximum (msec)	Peak Temperature (ev)	Peak Density (ρ/ρ_o)	Incident Pressure (kb)	Incident Temperature (ev)	Oscillation Frequency (cps)	Average Pressure (kb)	Average Temperature (ev)
1	20	8.2	0.92	2.5	28	0.70	1.0	420	0.42	8.0
1	40	0.75	5.6	0.56	28.2	0.09	0.32	67	0.055	3.0
0.1	20	3.3	0.24	8.6* 10.8	1.25	1.0	8.6	810	0.40	10.3
0.1	40	1.04	1.6	2.5** 2.9	3.1	0.084	1.1	160	0.0525	3.8
0.01	40	0.189	0.685	11.2	0.0432	0.10	11.2	(P) 380*** (T) 700	0.044	11.0

*First shock precedes radiation diffusion by only a little at first shock reflection raising wall temperatures to only 8.6 initially, but radiation further heated air near wall so that on fourth reflection temperature at the wall rose to 10.8 (See Fig. 25).

**After many reflection, the wall temperature rises toward an asymptotic value of nearly three electron volts (See Fig. 35).

***Although the cavity rapidly approaches a nearly isothermal state, the temperature seems to oscillate more than twice as rapidly as the pressure and density do - a consequence of the radiation dominance in this case.

but the imploding shock wave can be seen to grow in strength as it again approaches the origin. The shock is illustrated at times after the first reflection at the origin but before the second wall reflection in Fig. 7. At subsequent times, the interior of the cavity grows more nearly uniform in pressure, with relatively weak shocks batting back and forth.

Temperature profiles for the first case are shown prior to first reflection in Fig. 8 and at late times in Fig. 9. The high temperature gradient beyond 15 meters would undoubtedly not hold up for long under the influence of instabilities and mixing. Early and late density profiles are similarly illustrated in Figs. 10 and 11.

The early explosion history is dominated by radiation diffusion ahead of the bomb shock. For some distances the diffusion growth is faster than a shock wave at the same air temperature, but the diffusion growth slows as the driving temperature drops, and the rate of feeding energy into the radiation wave decreases. A shock wave gradually builds up at this front, and eventually dominates the expansion. Figure 12 illustrates this transition, showing the gradual increase of overdensity at the front. Times and radii are indicated for both the overdensity and the front temperature. Also shown is the interior temperature at corresponding times (but not as a function of the radius).

For the case of a 40 m cavity at normal density, the shock position versus time is shown in Fig. 13; and pressures, temperatures, and densities on the wall are given as functions of time in Figs. 14, 15, and 16, respectively. Again, the detailed shock structure is evident in these time histories at the wall, and are more obviously related to multiple shocks in the pressure profiles shown in Figs. 17, 18, and 19. Corresponding temperature profiles (Figs. 20 and 21) and density profiles (Figs. 22 and 23) continue to demonstrate the basic hydrodynamic nature of such a large cavity filled with normal air.

Pressure, temperature, and density at the wall are shown as functions of time for the 20 m cavity evacuated to one-tenth normal in Figs. 24,25, and 26. The wall pressures quickly damp towards an average value (Fig. 24) of slightly more than 400 atmospheres.

The damping of the reverberations may be in part due to the continued radiation flow demonstrated in Fig. 25. The rather rapid rise of wall temperature after the first reflection is a consequence of this continued heating. Pressure profiles show the same influence (Fig. 27) in the slow build-up of a shock and the rather low reflection factor (about 3.3). Late time pressure profiles show relatively small pressure fluctuations (Fig. 28). The temperature profiles for this case (Figs. 29 and 30) show the initial radiative dominance (Fig. 29), and the modest changes caused by shocks at late times (Fig. 30). Density profiles (Fig. 31) at early times appear to be quite complex, because of the slow development of the air shock, and the more dominant excursion of the bomb or case shock. The late time densities, however, become rather uniform (Fig. 32).

For the larger (40 m) cavity at one-tenth normal air density, Fig. 33 shows a plot of shock positions as a function of time, while Fig. 34 describes the wall pressure versus time for many reverberations. With less air in the cavity, the radiation continues to diffuse, and Fig. 35 shows its influence superimposed on the shock effects on wall temperature. A corresponding but opposite drift must exist in the air densities near the wall, since the pressures at the wall exhibited no obvious change from the inter-cycle average, and it does show in Fig. 36. The pressure profiles for this case (40m, 1/10th normal) show some of the irregularities introduced by secondary shocks as well as the progress of the main air shock and its reflections (Figs. 37 and 38).

The temperature profiles of Figs. 39 and 40 show features similar to the corresponding plots for the normal density case (Figs. 20 and 21), but with smaller temperature gradients sustained for shorter times. The density profiles (Figs. 41 and 42) show the shock forming at a larger radius than in the normal density case (Figs. 22 and 23) but, in keeping with the temperature differences, developing a shallower fireball. In this case, the interior densities are mostly greater than one-fifth of the initial ambient cavity density, while in the previous example with normal density air, the fireball interior drops to less than one-tenth of the initial ambient value.

When the 40 m cavity is pumped down to one-hundredth normal, the phenomena at the wall changes character. The wall first sees the radiation diffusion wave, and the wall pressure (Fig. 43) as well as temperature (Fig. 44) show a slow rise over the first half millisecond before the shock strikes the wall. Actually, the radiation front is slowing down and beginning to shock up, so that the density at the wall shows some slight rise before shock arrival (Fig. 45). Perhaps more interesting, however, is the extra oscillation that persists in the temperature profiles. Every other pulse in Fig. 44 (wall temperature versus time) corresponds to the shock reflection, but the comparable temperature pulses in between have apparently no accompanying consequence in either the pressure or the density. Of course, there must be some consequence, but the temperature variations are not large to begin with, and the shocks are nearly isothermal.

The pressure profiles for this case show the diffusion front preceding the shock wave all the way to the wall (Fig. 46). The subsequent reflected shocks are quite weak (Fig. 47) except as they implode on the origin each time. The temperature profiles shown in Figs. 48 and 49 show that after the initial diffusion growth fills the cavity, the air becomes quite transparent and forces an isothermal condition even through the shocks - rising and falling uniformly and only slightly as the shock strikes the wall and then the origin.

In contrast, the density profiles of Figs. 50 and 51 show the gradients in density which travel with the isothermal shock, indicating the persistence of the reverberations even under these radiatively transparent conditions.

The final figure (Fig. 52) is a composite of several curves which describe the transition from radiative growth to shock growth for the fireball in the one-tenth normal atmosphere. The shock density development is illustrated by the curve labeled $(10\eta - 1)$, which is the same as the compression, or the shock overdensity divided by the initial ambient density. This curve suggests that a shock begins to form by 12 m ($\sim$ 30 μsec) but is not fully formed until 21 m (250 μsec). The growth here should be compared with that shown in Fig. 12 for normal density air.

The temperature at this same front is also shown. It drops most rapidly, of course, at the time that the compression rises the fastest. The inner temperature of the nearly isothermal fireball is shown as a function of the time only. The compression in the bomb or case shock is also shown, but not at the same time scale as used for the air shock compression curve, since at corresponding times, the bomb shock is still inside and behind the main shock until the time of catch-up (before 200 μsec).

REFERENCES

1. Latter, A.L., R.E. LeLevier, E.A. Martinelli, and W.G. McMillan, J. Geophys. Research, Vol. 66, March 1961, pp. 943-946.

2. Herbst, R.F., G.C. Werth, and D.L. Springer, J. Geophys. Research, Vol. 66, March 1961, pp. 959-978.

3. Latter, A.L., E.A. Martinelli, J. Mathews, and W.G. McMillan, J. Geophys. Research, Vol. 66, September 1961, pp. 2929-2936.

4. Haskell, N.A., J. Geophys. Research, Vol. 66, September 1961, pp. 2937-2944.

5. Murphey, B.F., J. Geophys. Research, Vol. 66, March 1961, pp. 947-958.

6. Adams, W.M., and L.M. Swift, Geophysics, Vol. 26, December 1961, pp. 765-771.

7. Adams, W.M., and D.C. Allen, Geophysics, Vol. 26, December 1961, pp. 772-799.

8. Johnson, G.W., G.H. Higgens, and C.E. Violet, J. Geophys. Research, Vol. 64, October 1959, pp. 1457-1470.

9. Adams, W.M., R.G. Preston, P.L. Flanders, D.C Sachs, and W.R. Perret, J. Geophys. Research, Vol. 66, March 1961, pp. 903-942.

10. Brode, H.L., Theoretical Description of the Blast and Fireball for a Sea Level Kiloton Explosion (U), The RAND Corporation, RM-2246, June 1965 (Confidential).

11. Brode, H.L., Nuclear Blast Calculations (U), The RAND Corporation, RM-4457-PR, March 1965 (Secret-Restricted Data).

12. Brode, H.L., and B.R Parkin, J. Geophys. Research, Vol. 68, May 1, 1963, pp. 2761-2789.

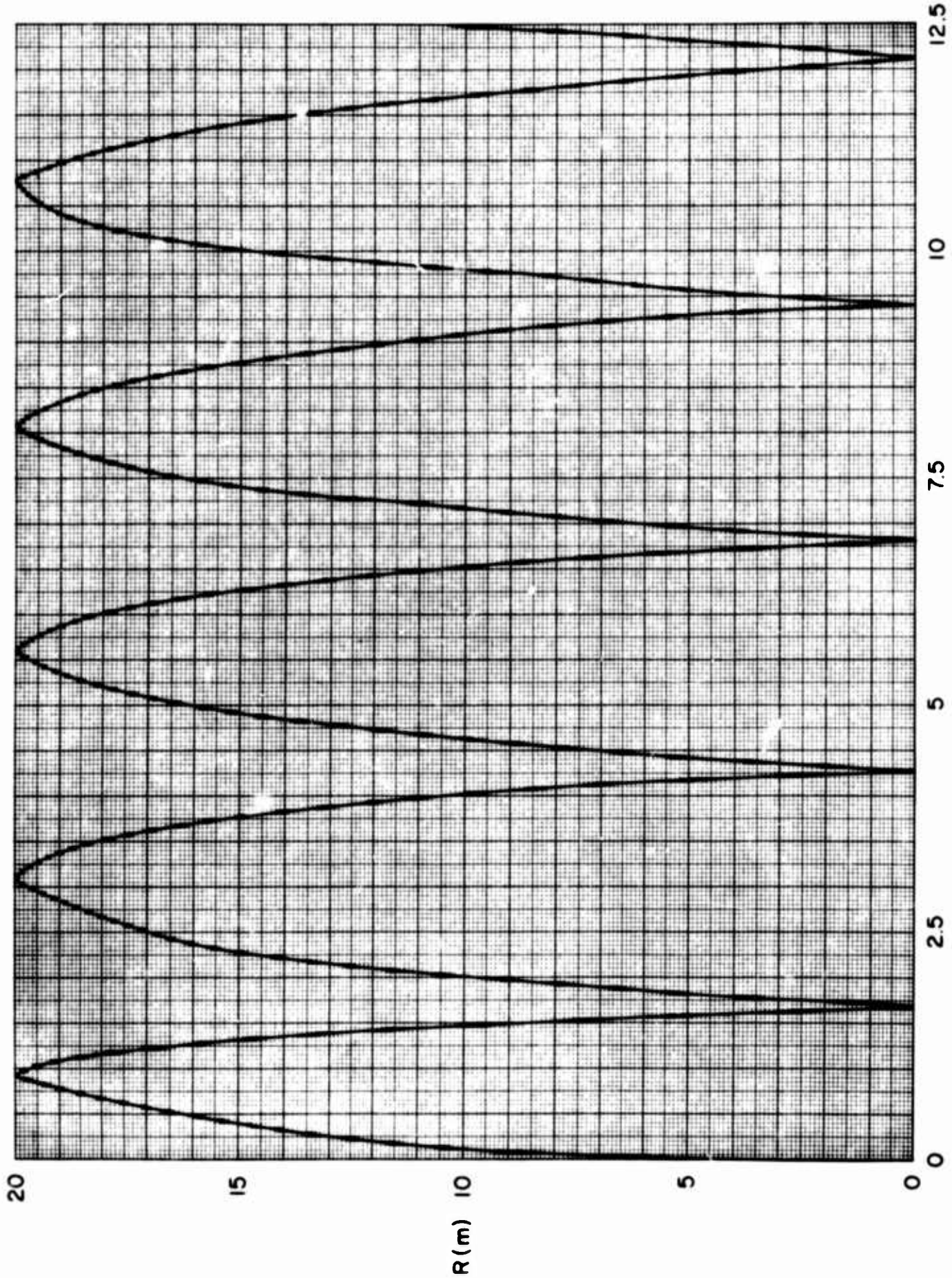

Fig. 1—Shock position versus time, $\rho_i = \rho_0$

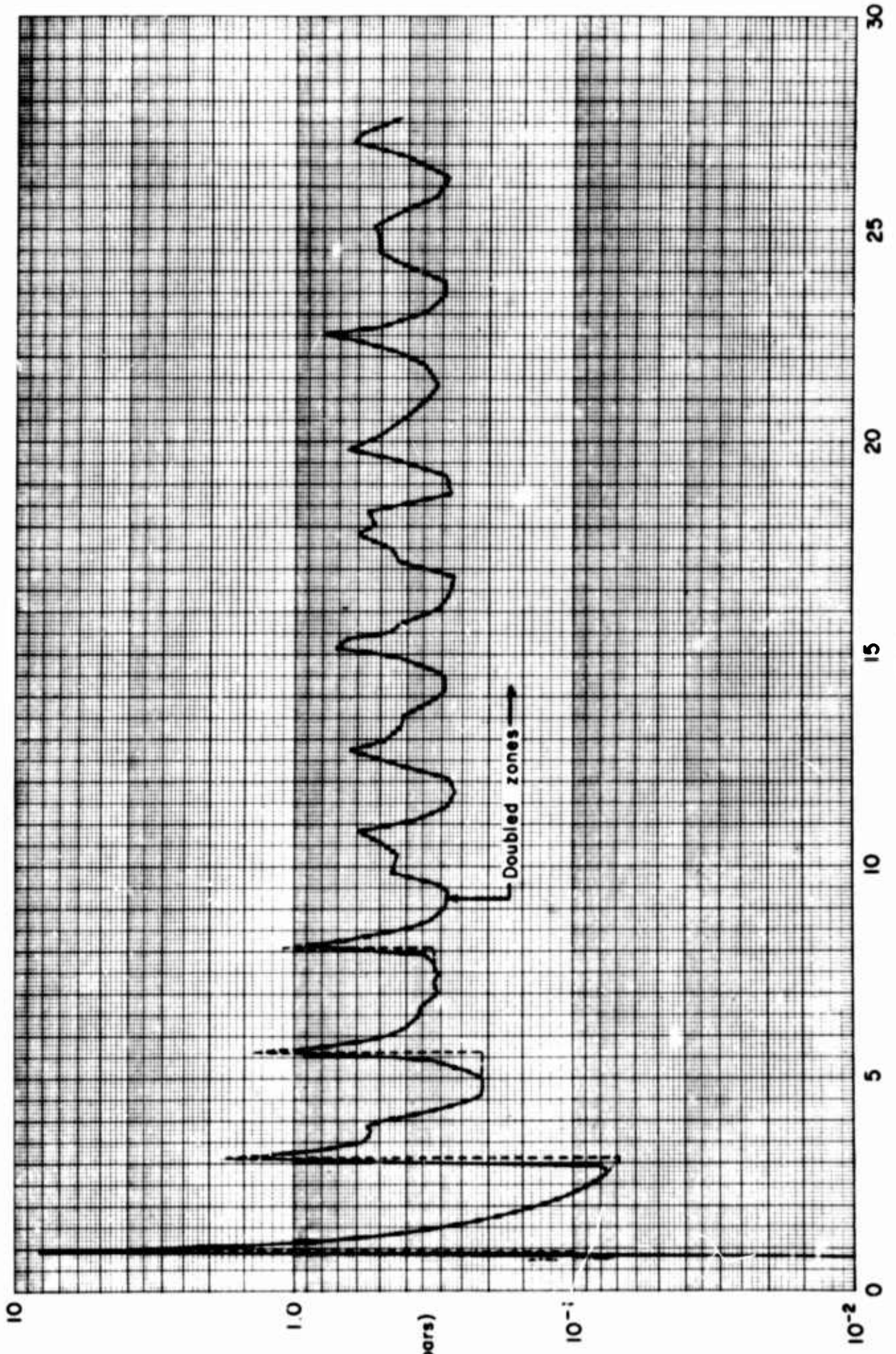

Fig. 2—Wall pressure versus time, 20 m cavity, $\rho_i = \rho_0$

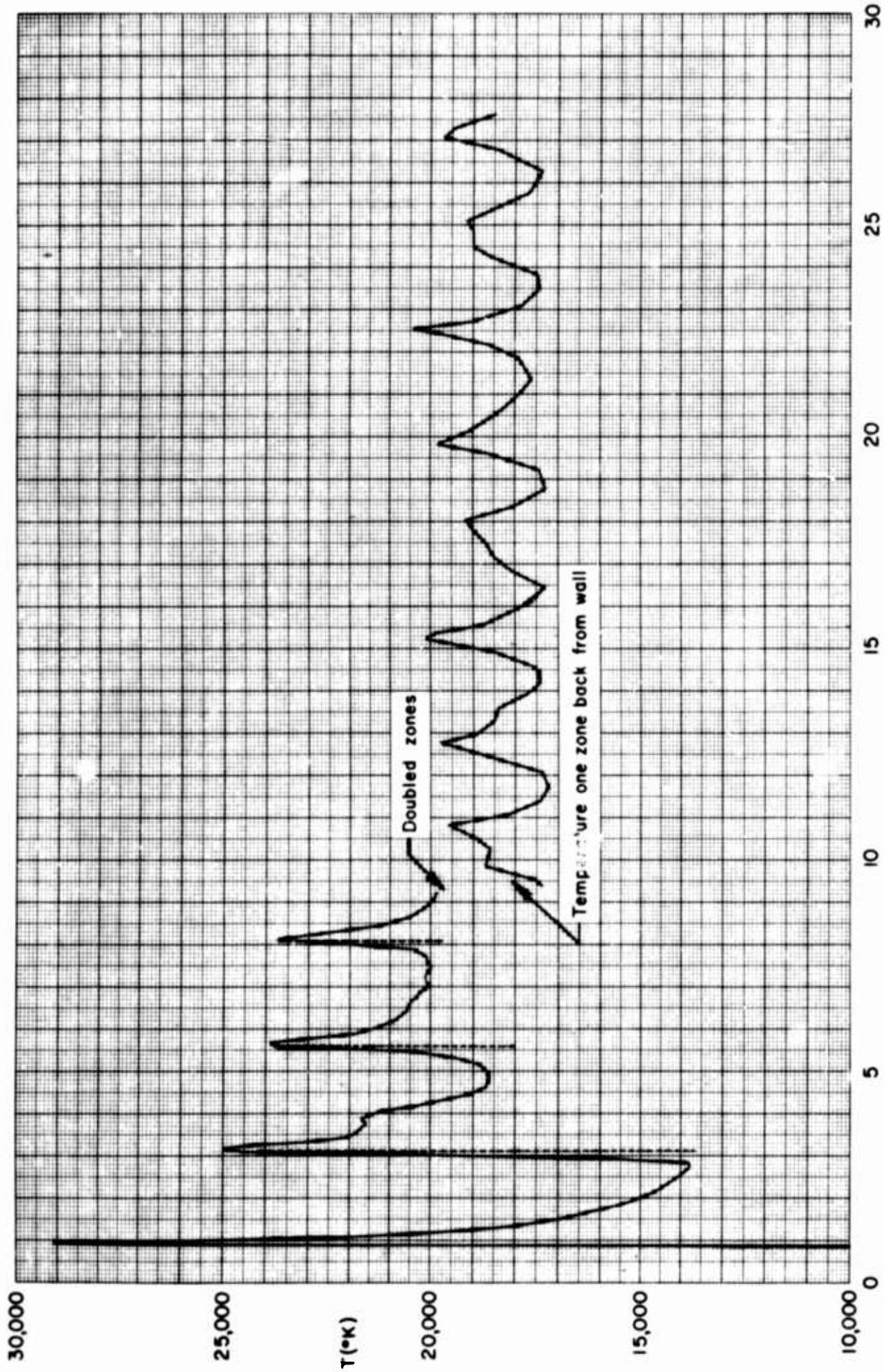

Fig. 3—Wall temperature versus time, 20 m cavity, $\rho_1 = \rho_0$

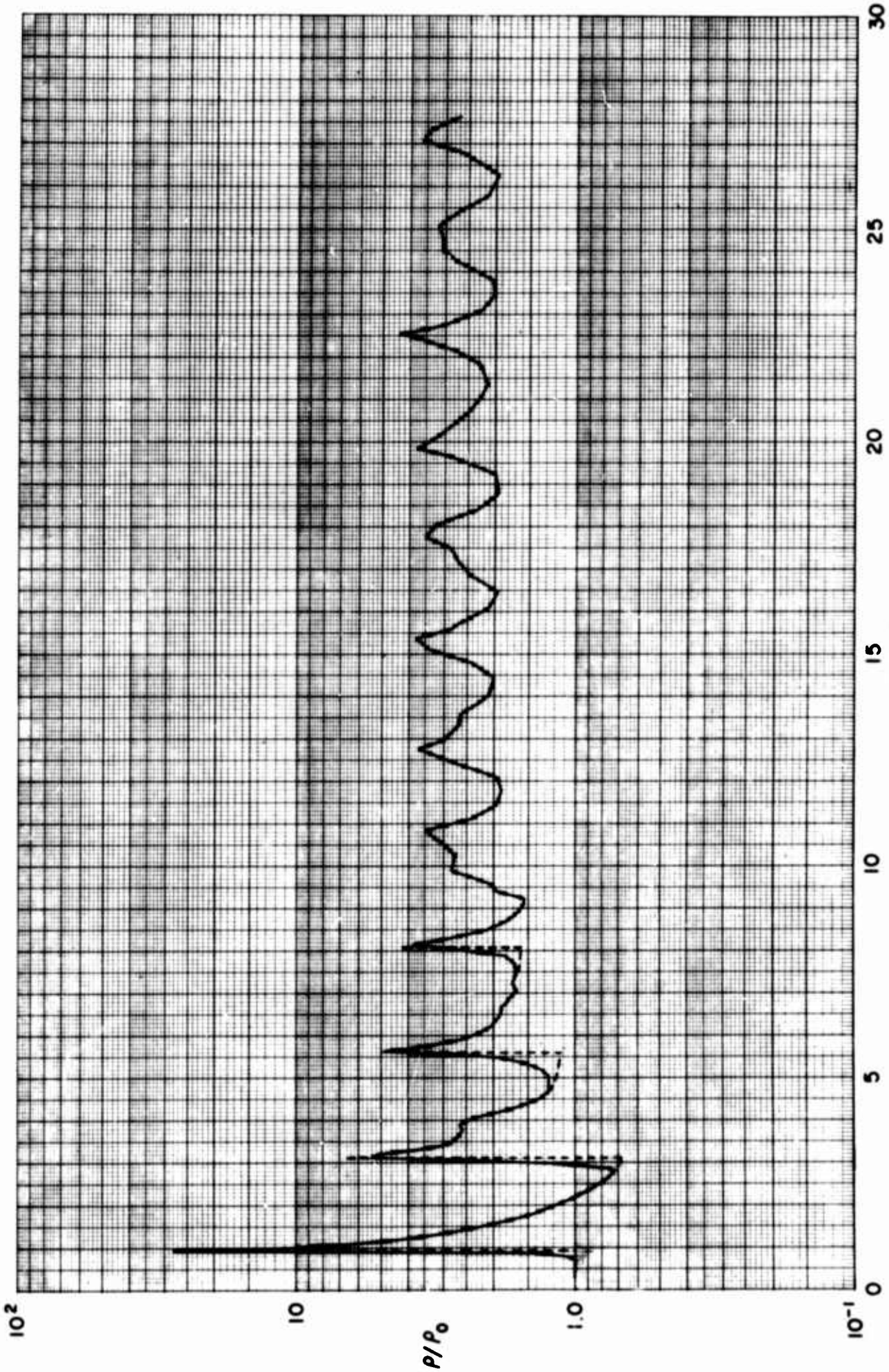

Fig. 4—Wall density ratio versus time, 20 m cavity

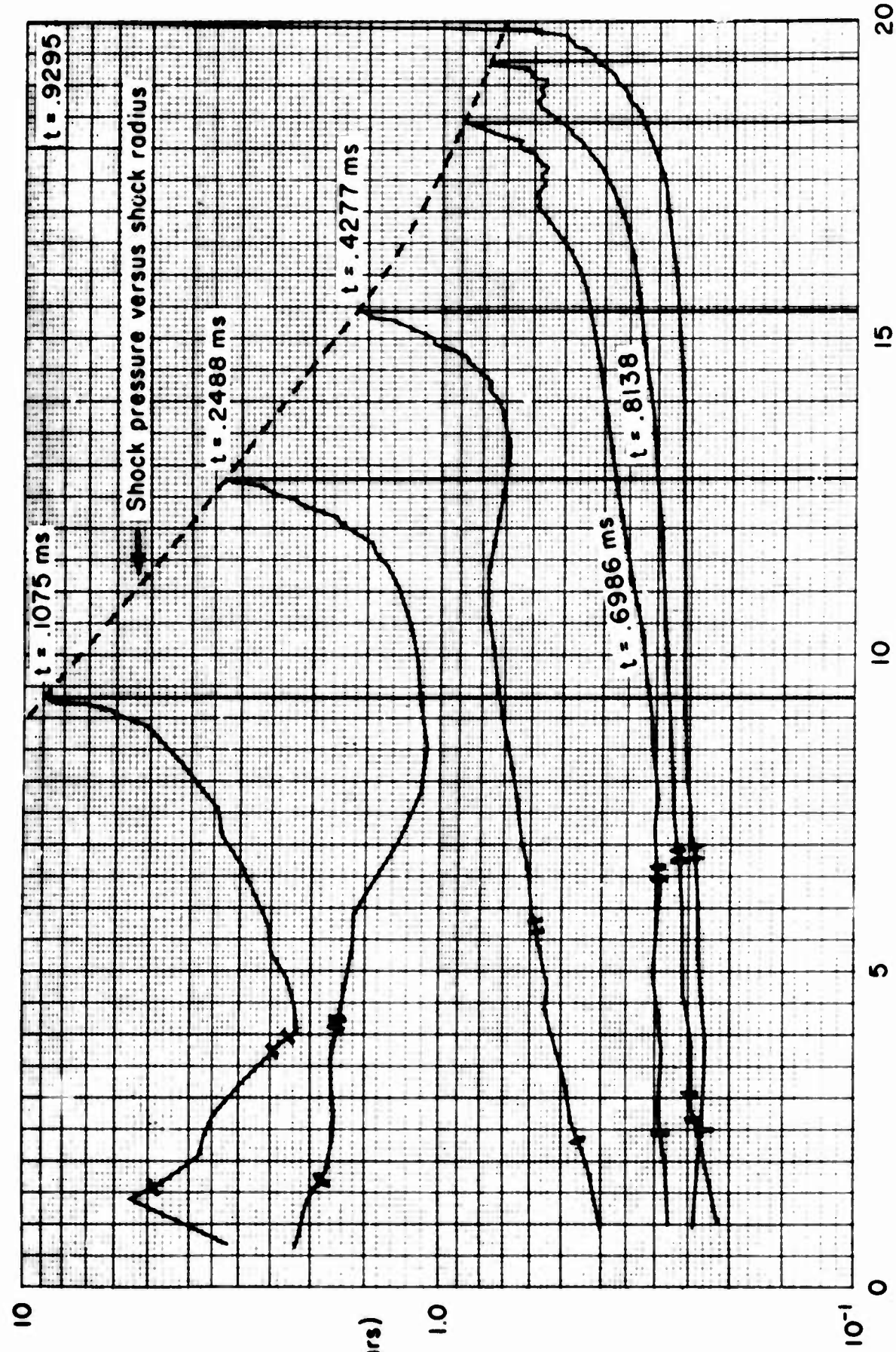

Fig. 5—Pressure profiles at times before first reflection, $\rho_i = \rho_0$

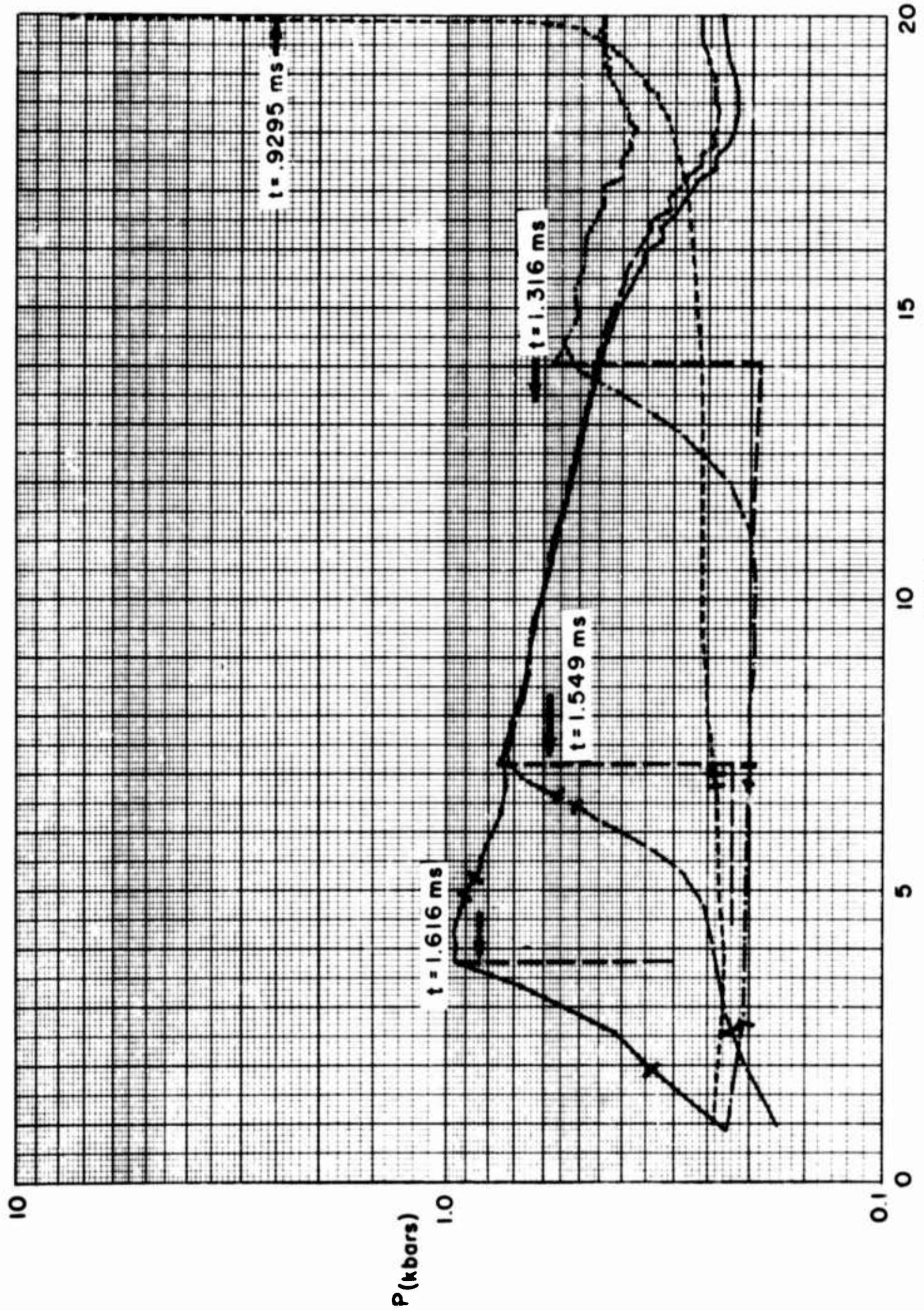

Fig. 6—Pressure profiles at times after first reflection, $\rho_i = \rho_0$

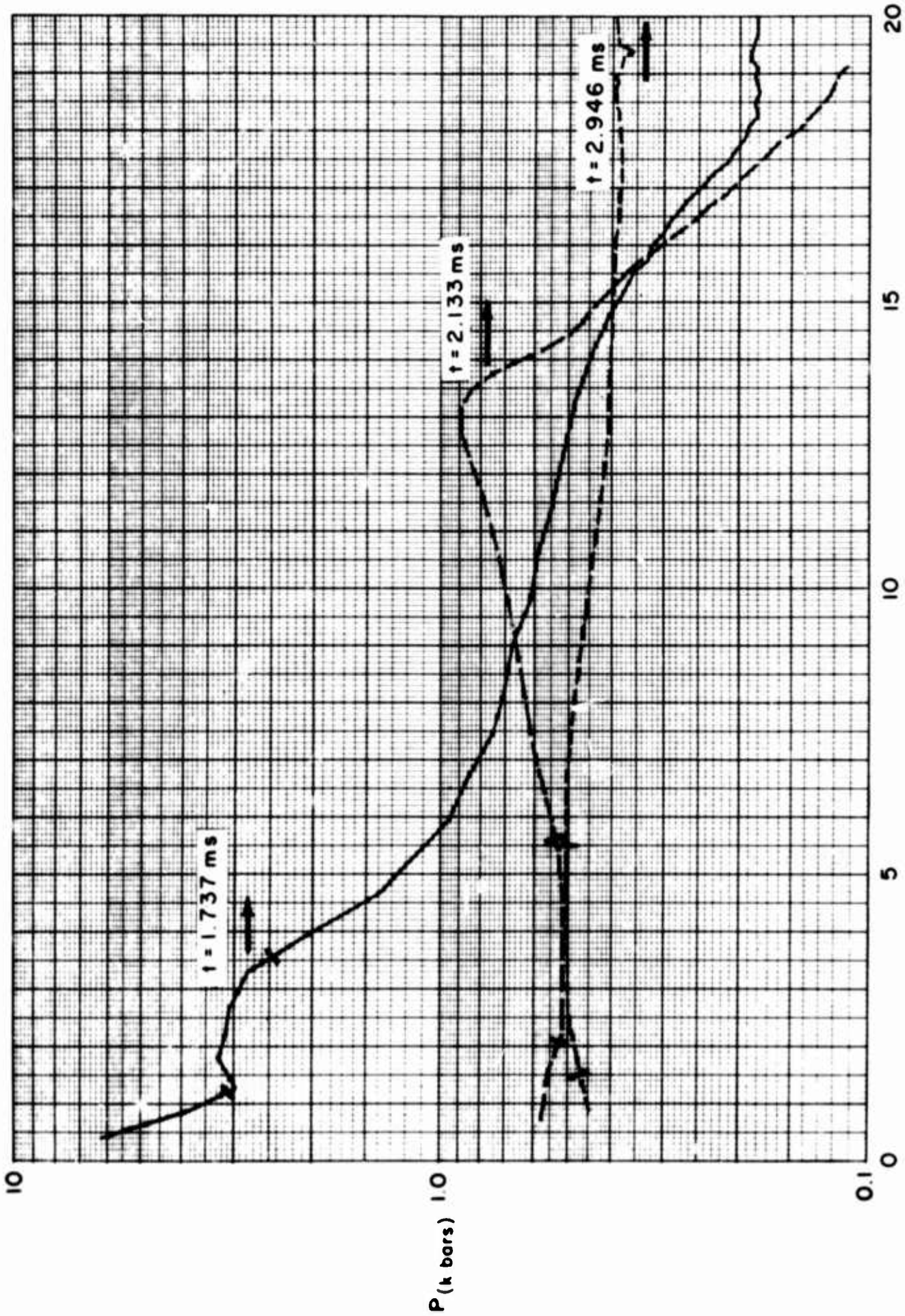

Fig. 7—Pressure profiles at times before second wall reflection, $\rho_i = \rho_0$

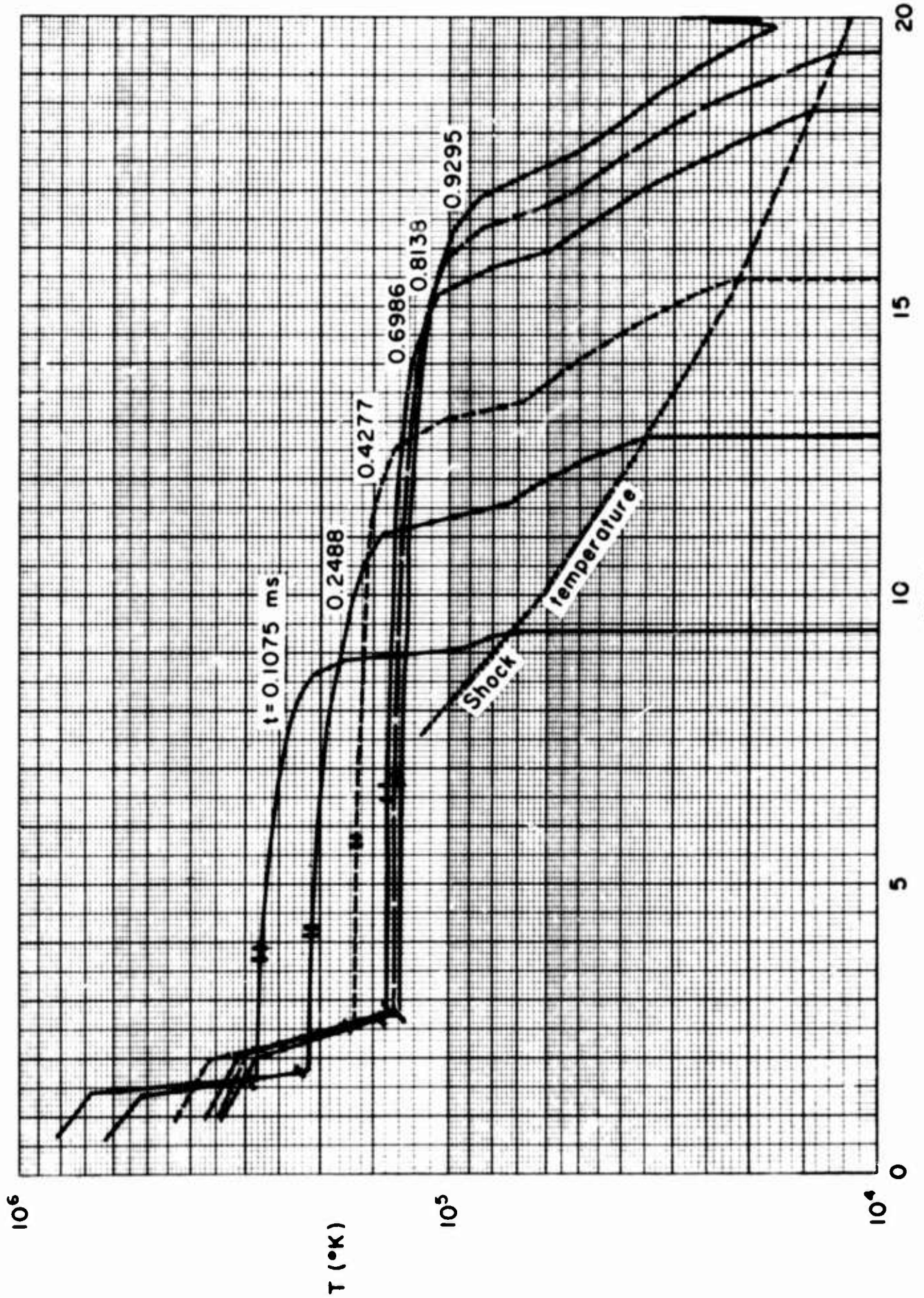

Fig. 8—Temperature profiles at times before first reflection, $\rho_i = \rho_0$

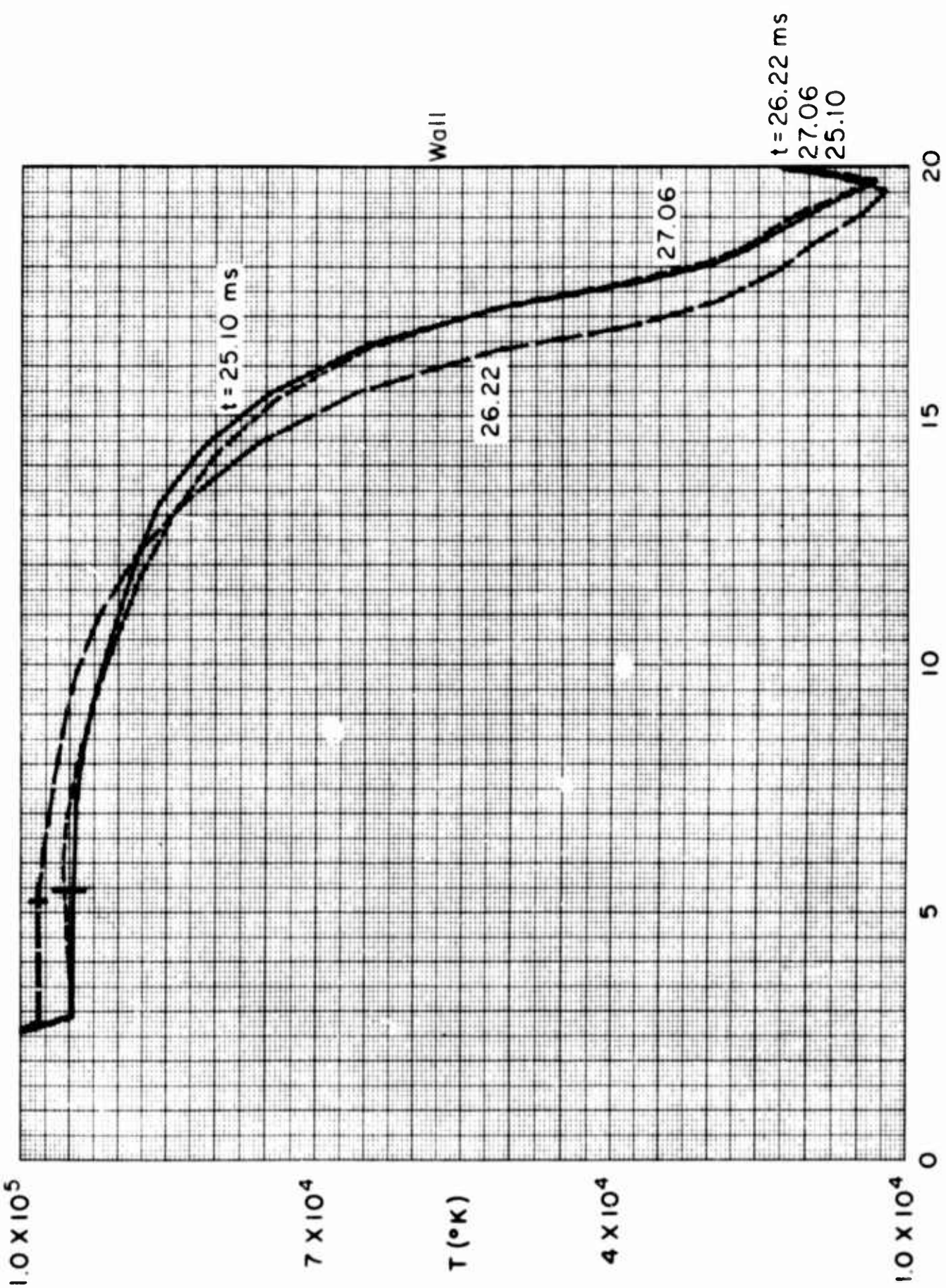

Fig. 9—Temperature profiles at late times (after many reflections), $\rho_i = \rho_0$

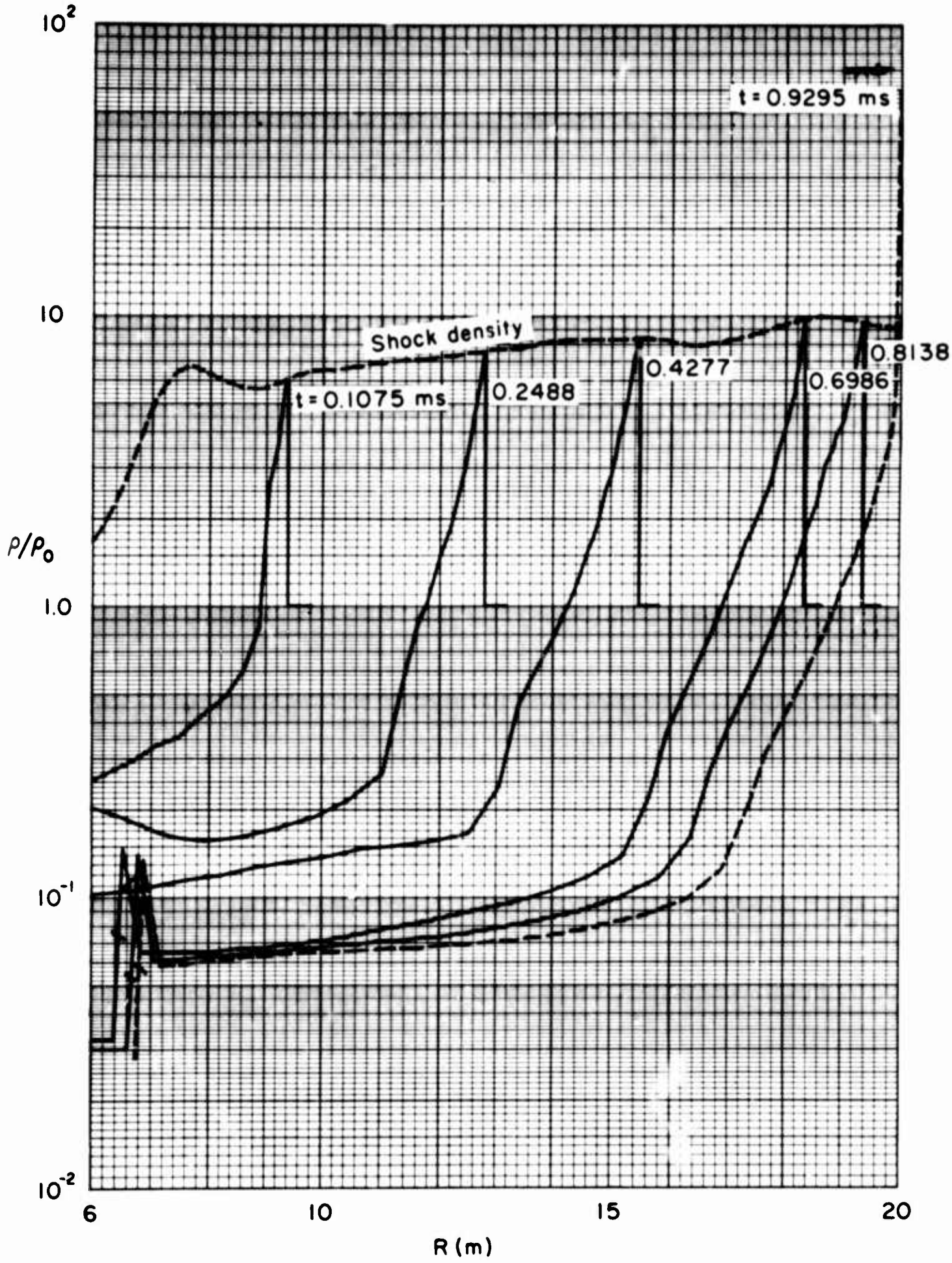

Fig. 10—Density profiles at early times (before reflection) $\rho_i = \rho_0$

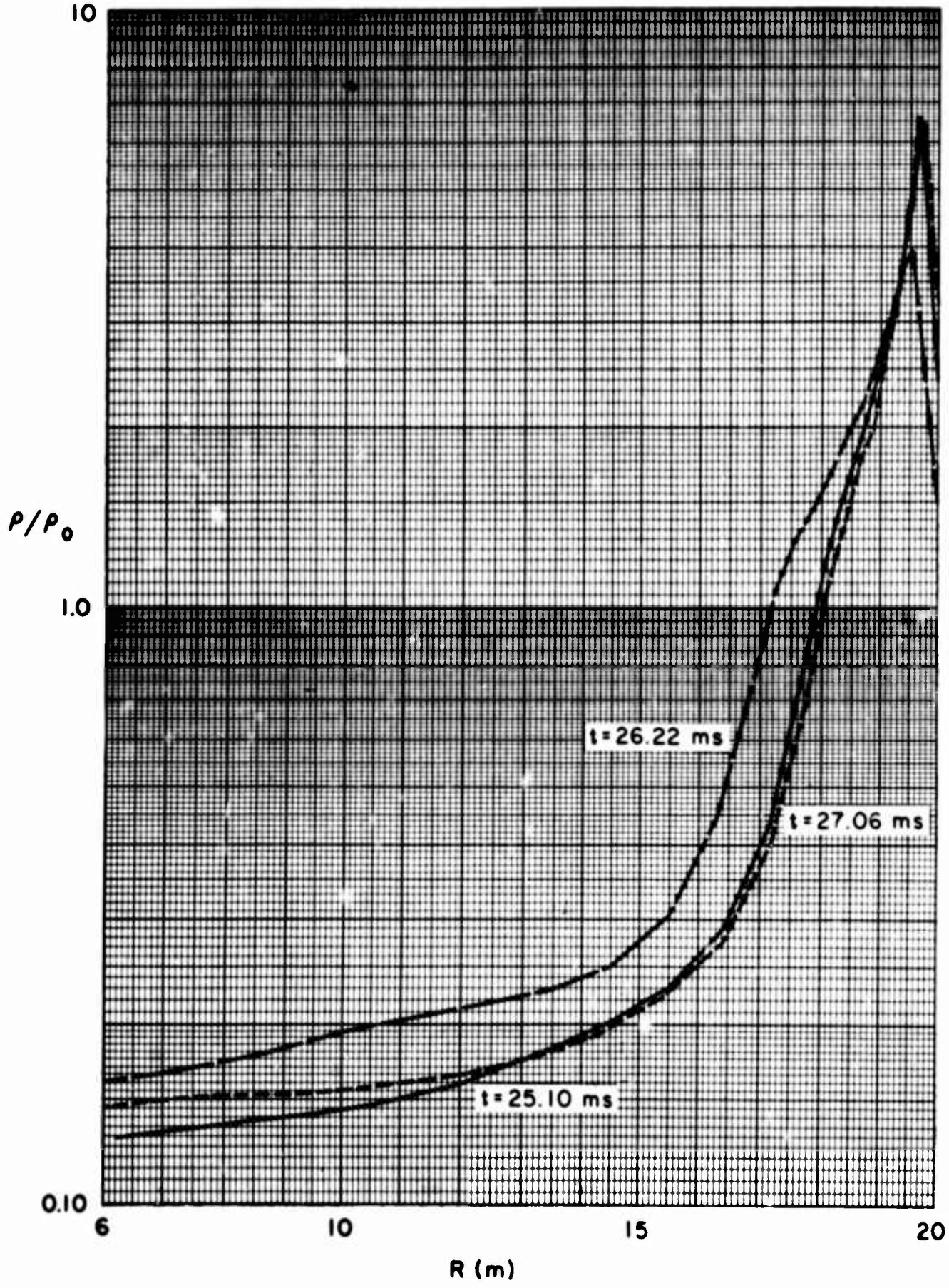

Fig. 11—Late density profiles (after many reflections) $\rho_i = \rho_0$

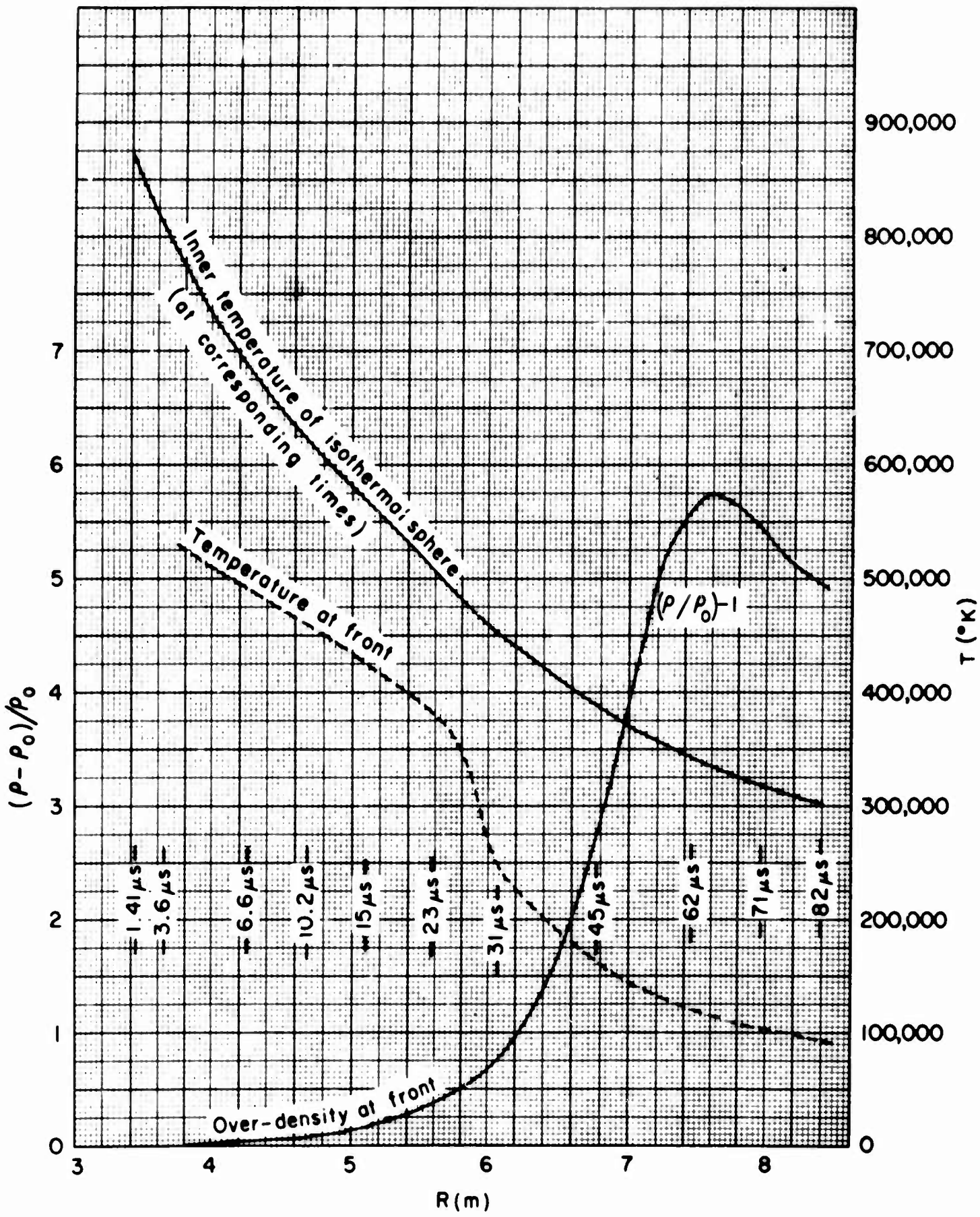

Fig. 12—Radiation diffusion—shock-wave transition

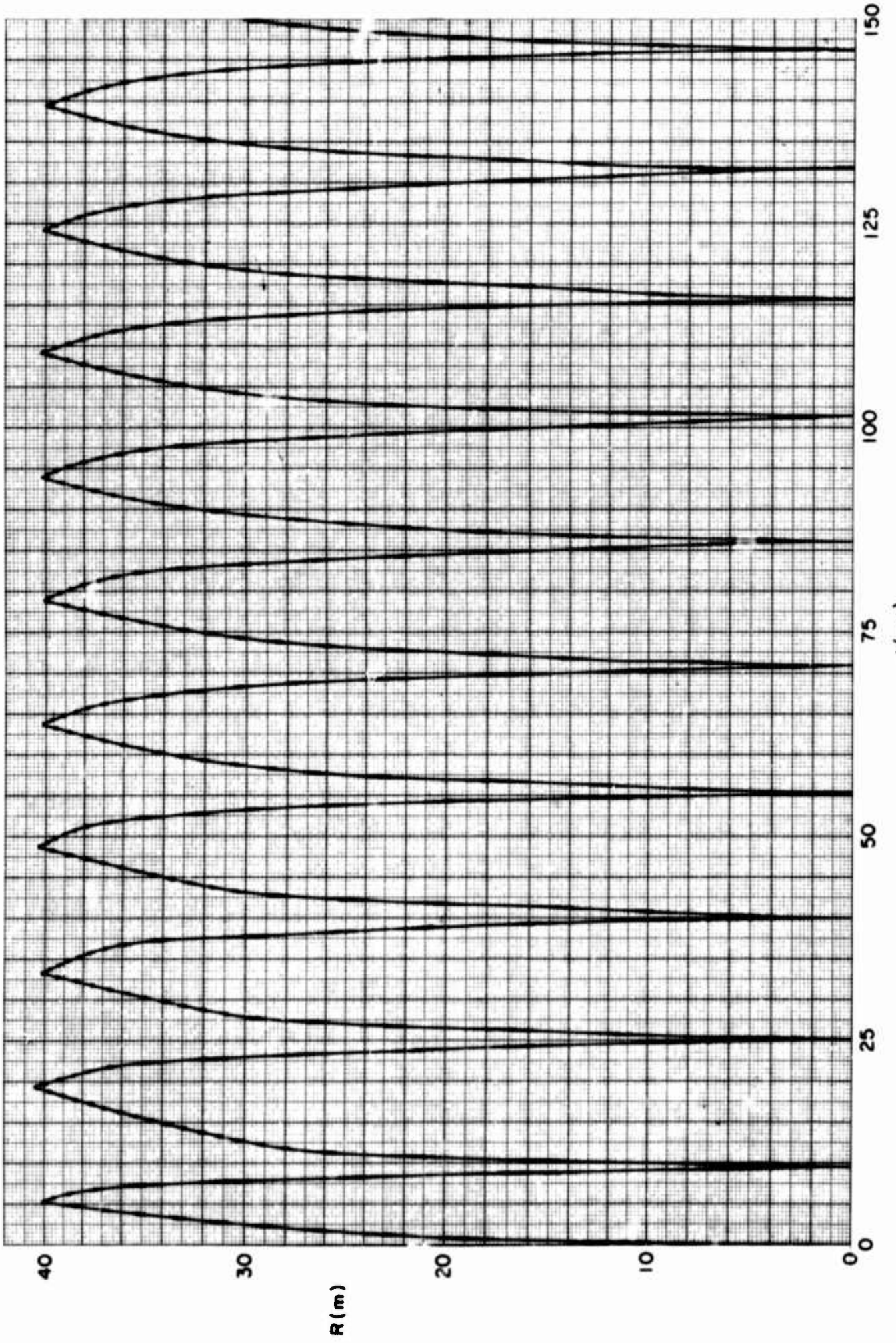

Fig. 13—Shock radius versus time for 40 m cavity, $\rho_i = \rho_0$

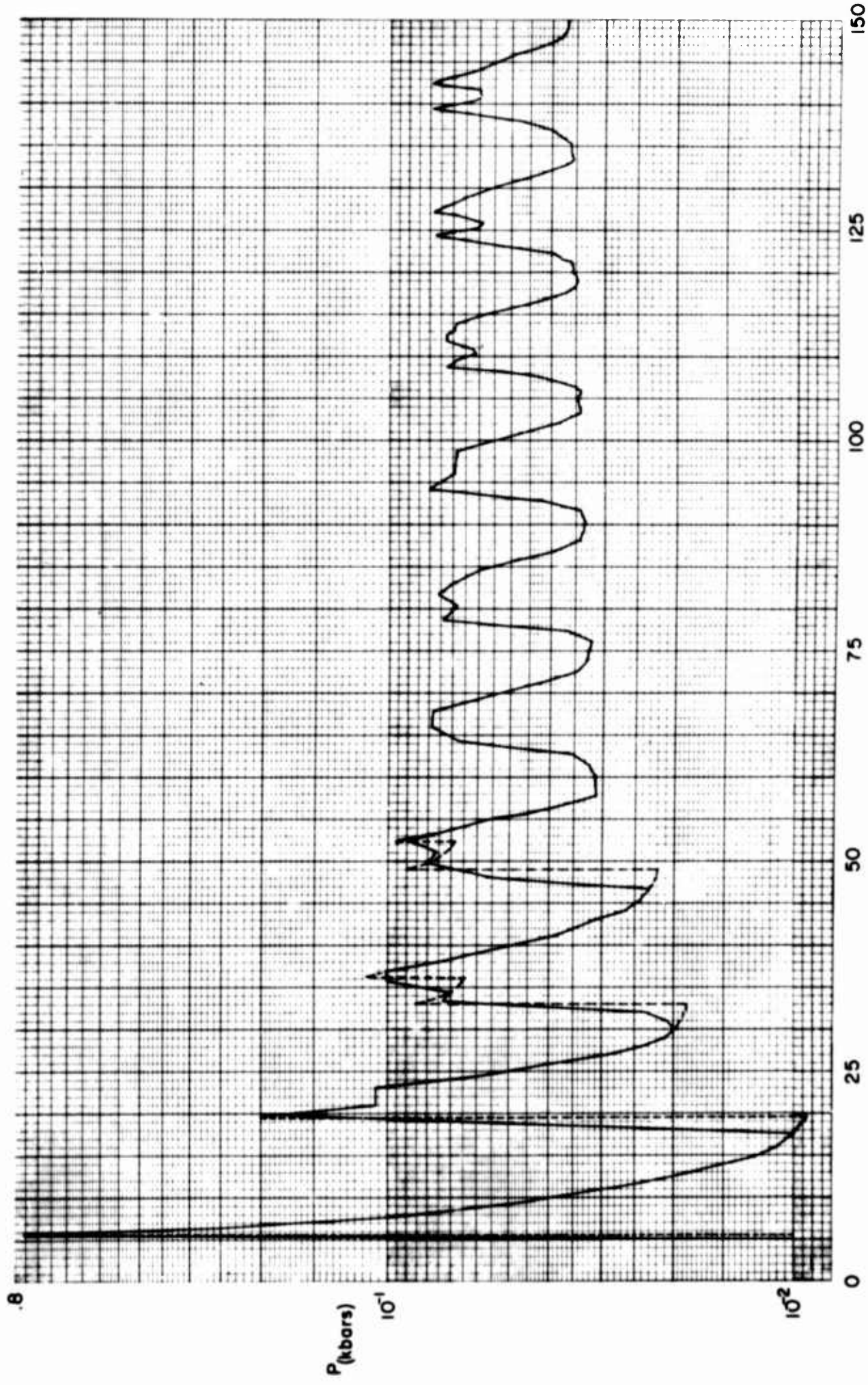

Fig. 14—Wall pressure versus time for 40 m cavity, $\rho_i = \rho_0$

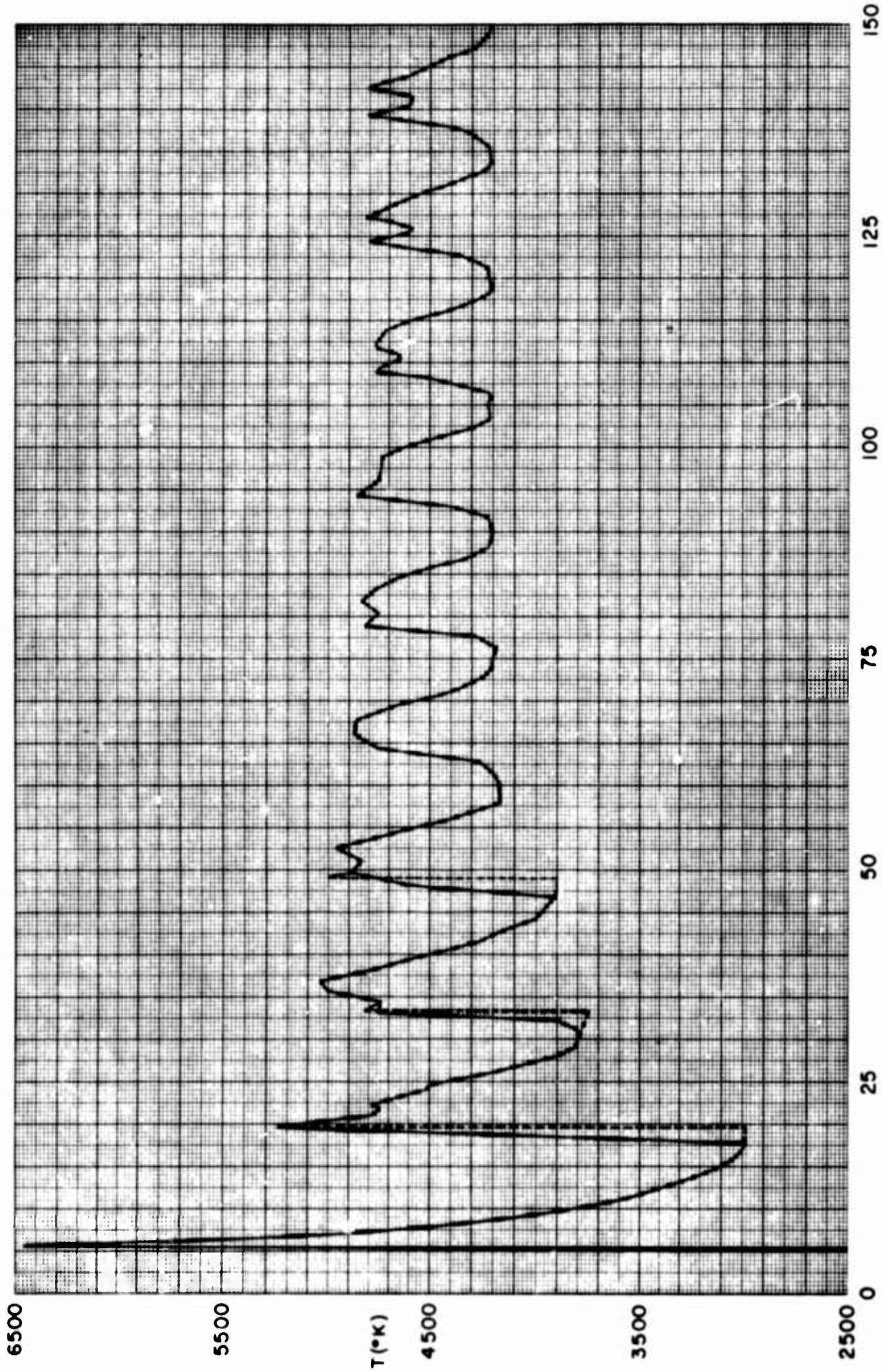

Fig. 15—Wall temperature versus time for 40 m cavity, $\rho_i = \rho_0$

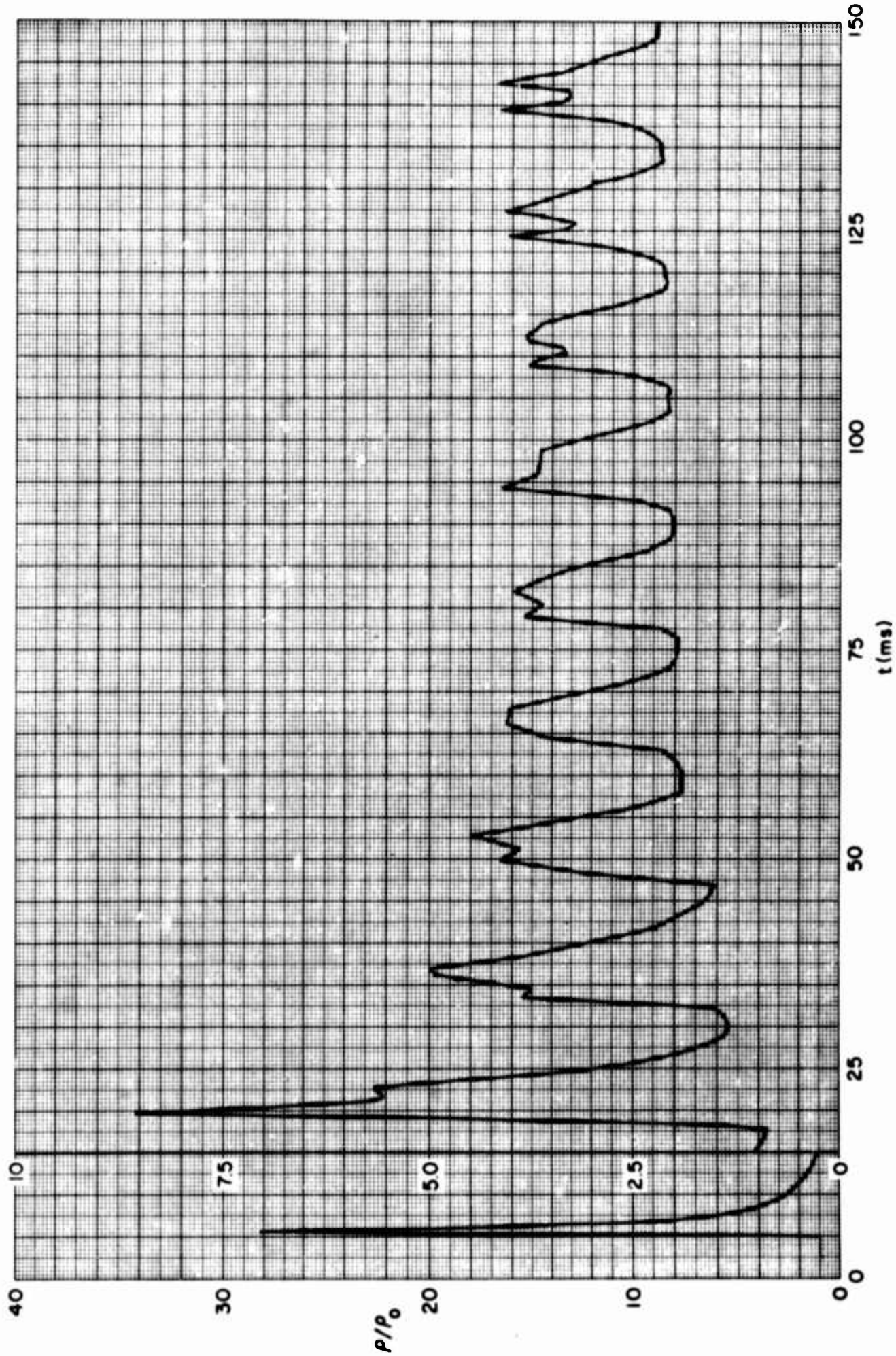

Fig. 16— Wall density versus time for 40 m cavity, $\rho_i = \rho_0$

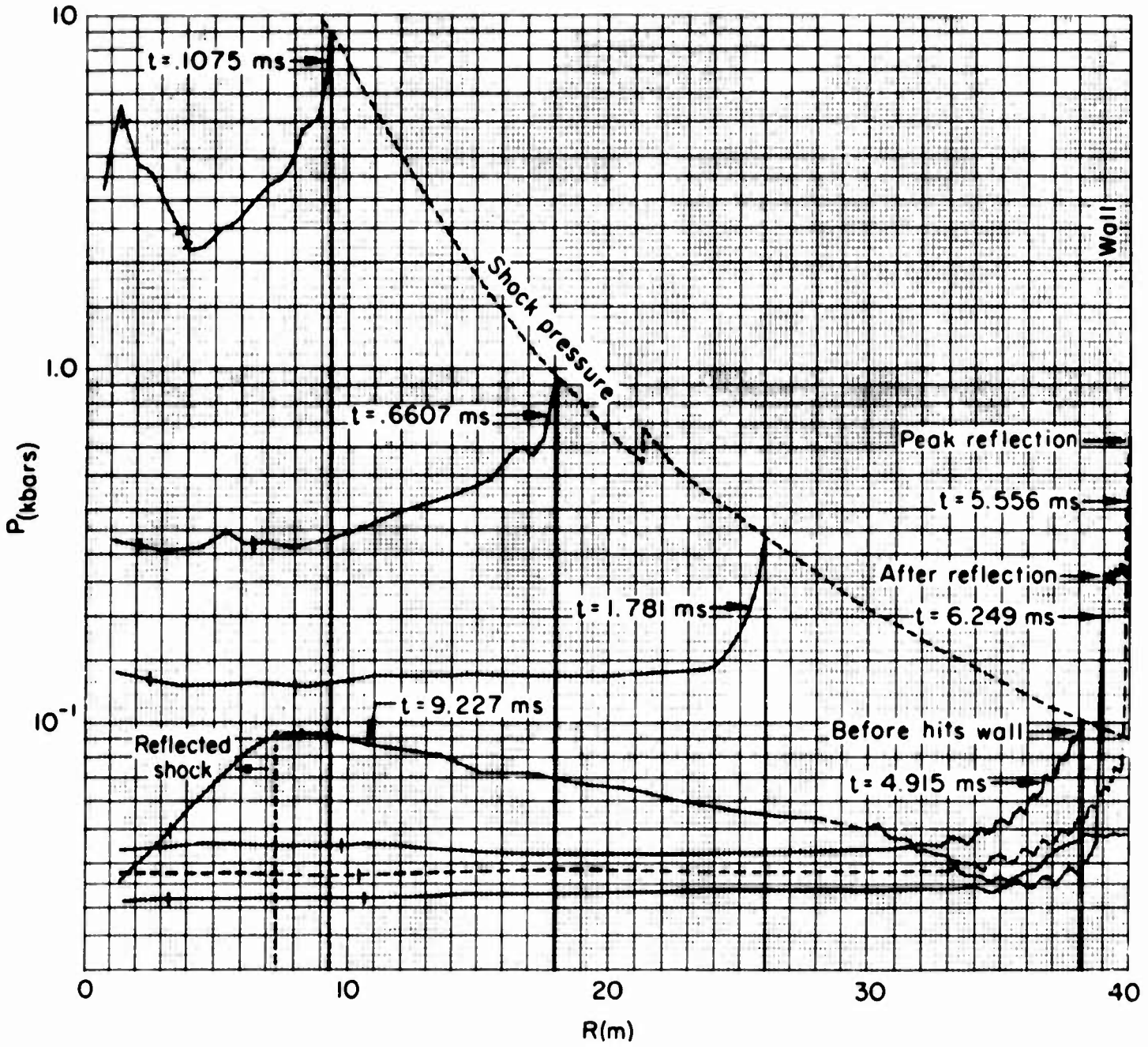

Fig. 17—Pressure versus radius before and after first reflection, $\rho_i = \rho_0$

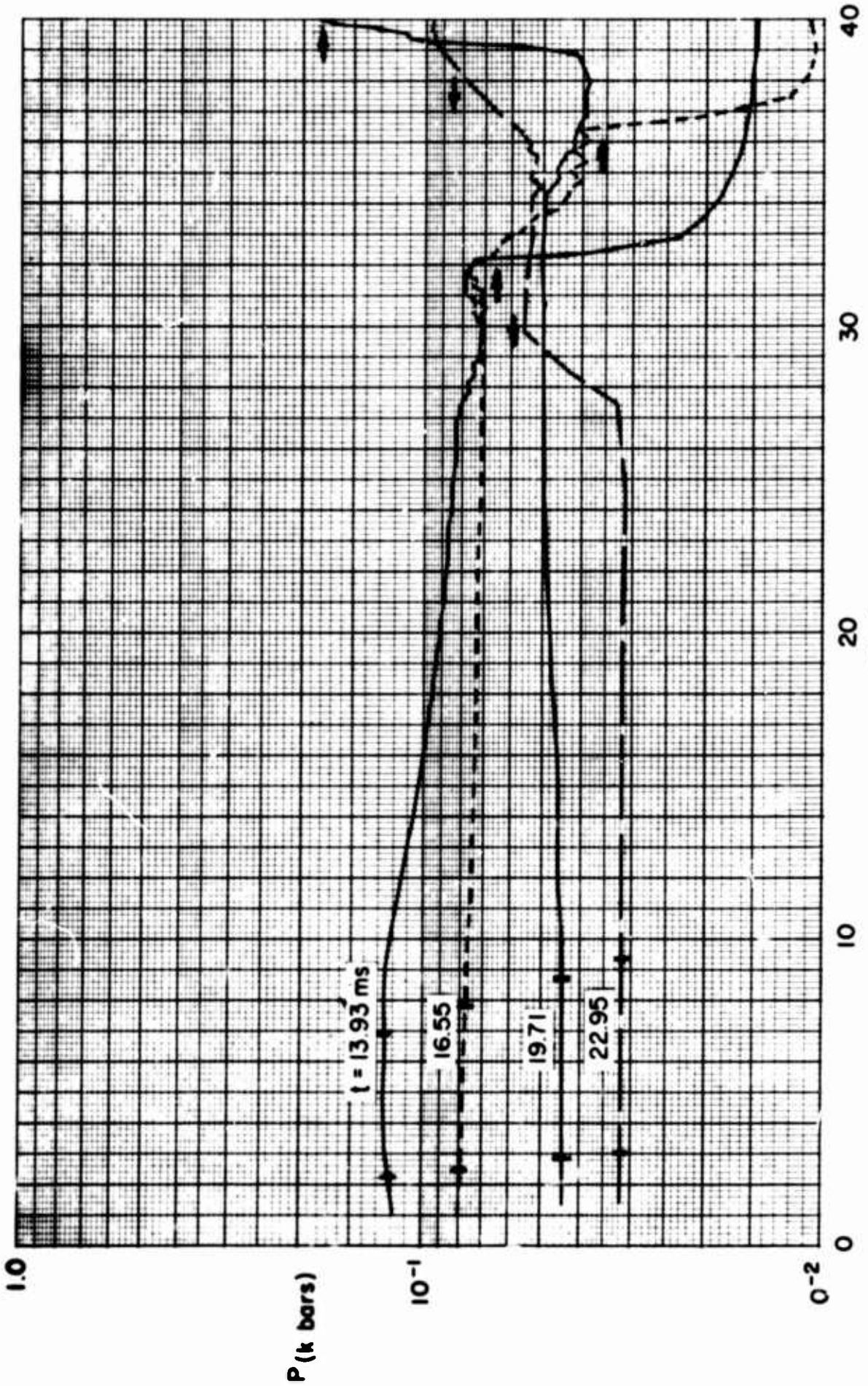

Fig. 18—Pressure profiles at times between first and second reflections, $\rho_i = \rho_0$

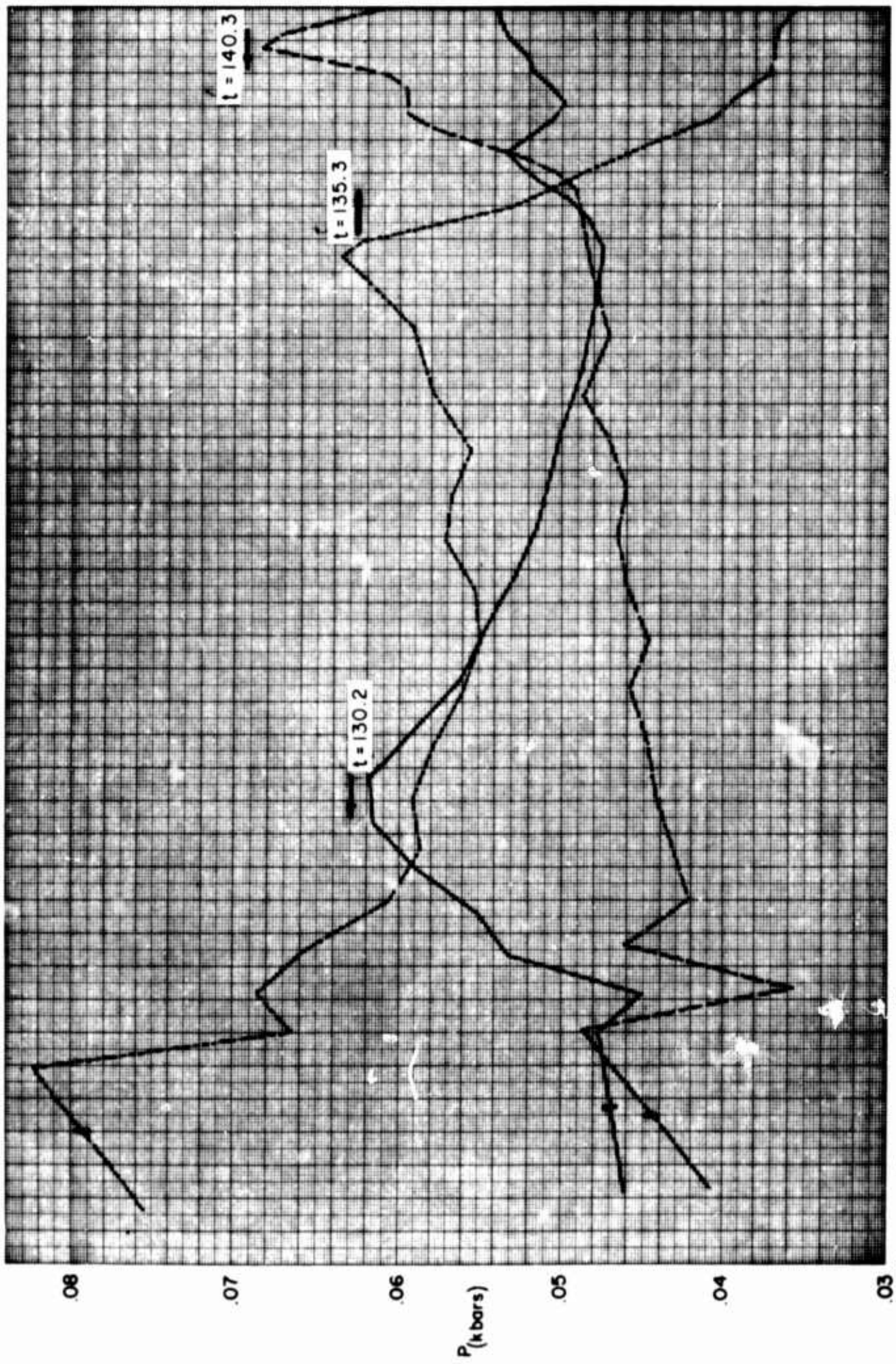

Fig. 19—Pressure profiles at late times, $\rho_i = \rho_0$

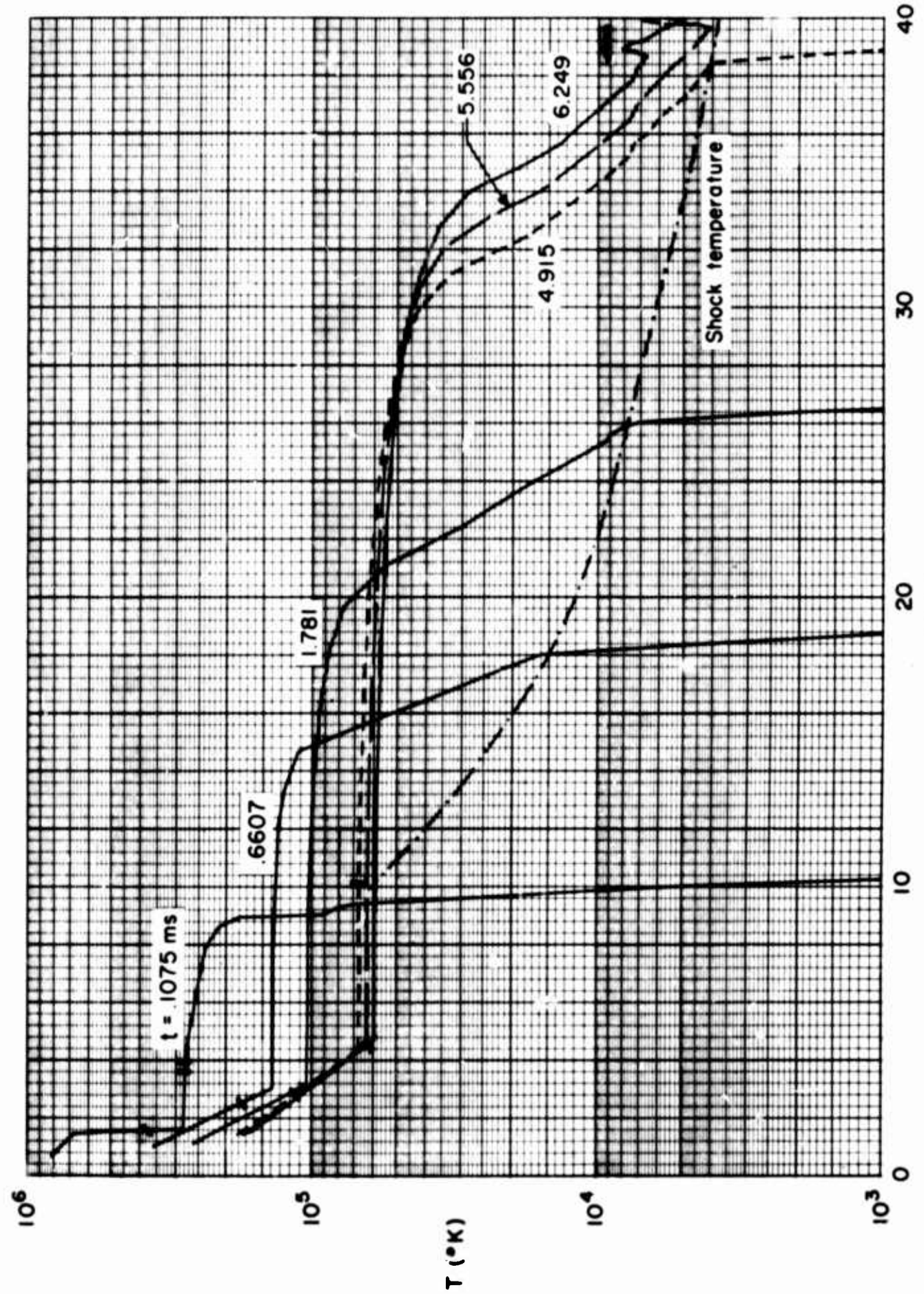

Fig. 20—Temperature profiles at times before first reflection, $\rho_i = \rho_0$

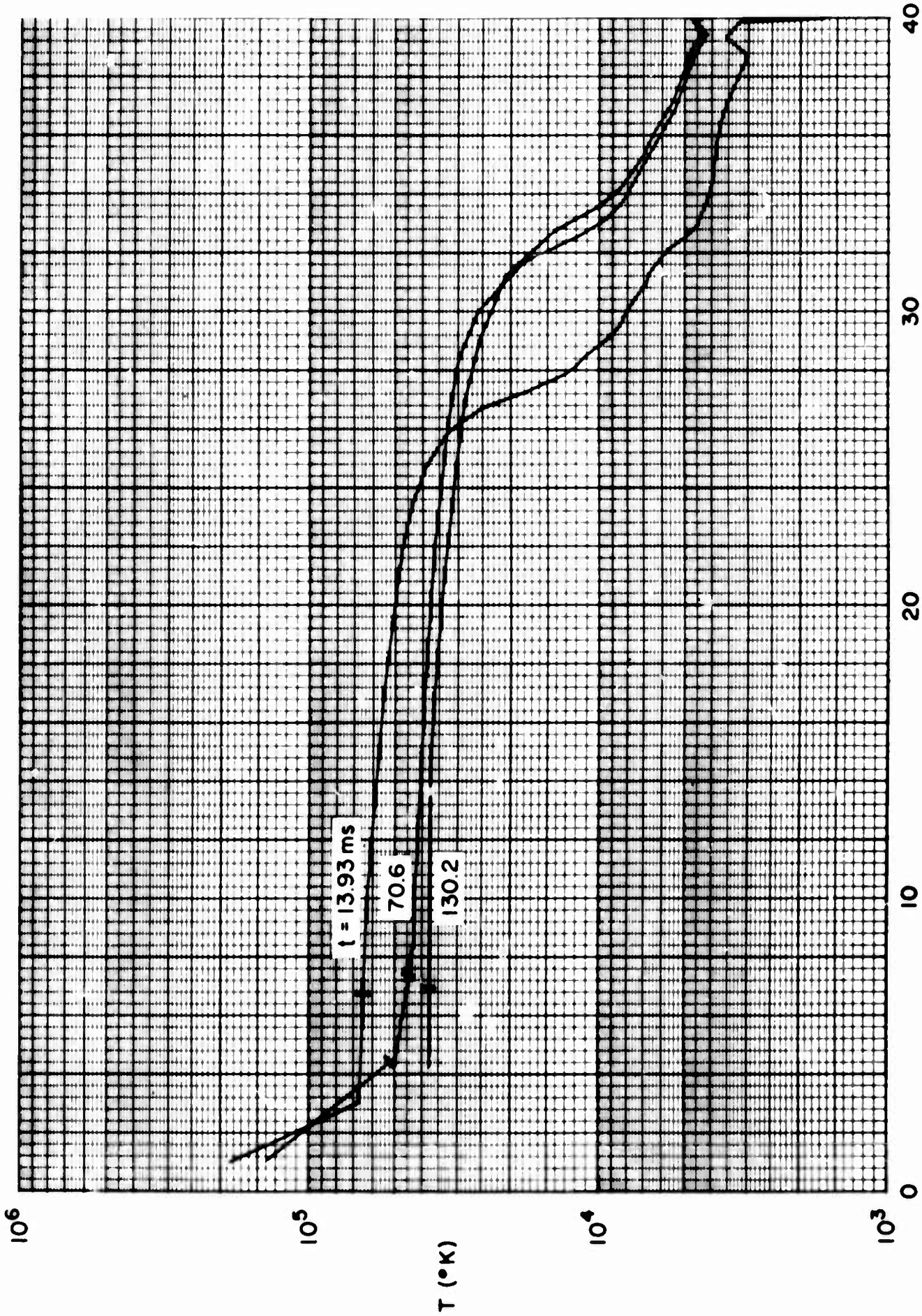

Fig. 21—Temperature profiles after first reflection, $\rho_i = \rho_0$

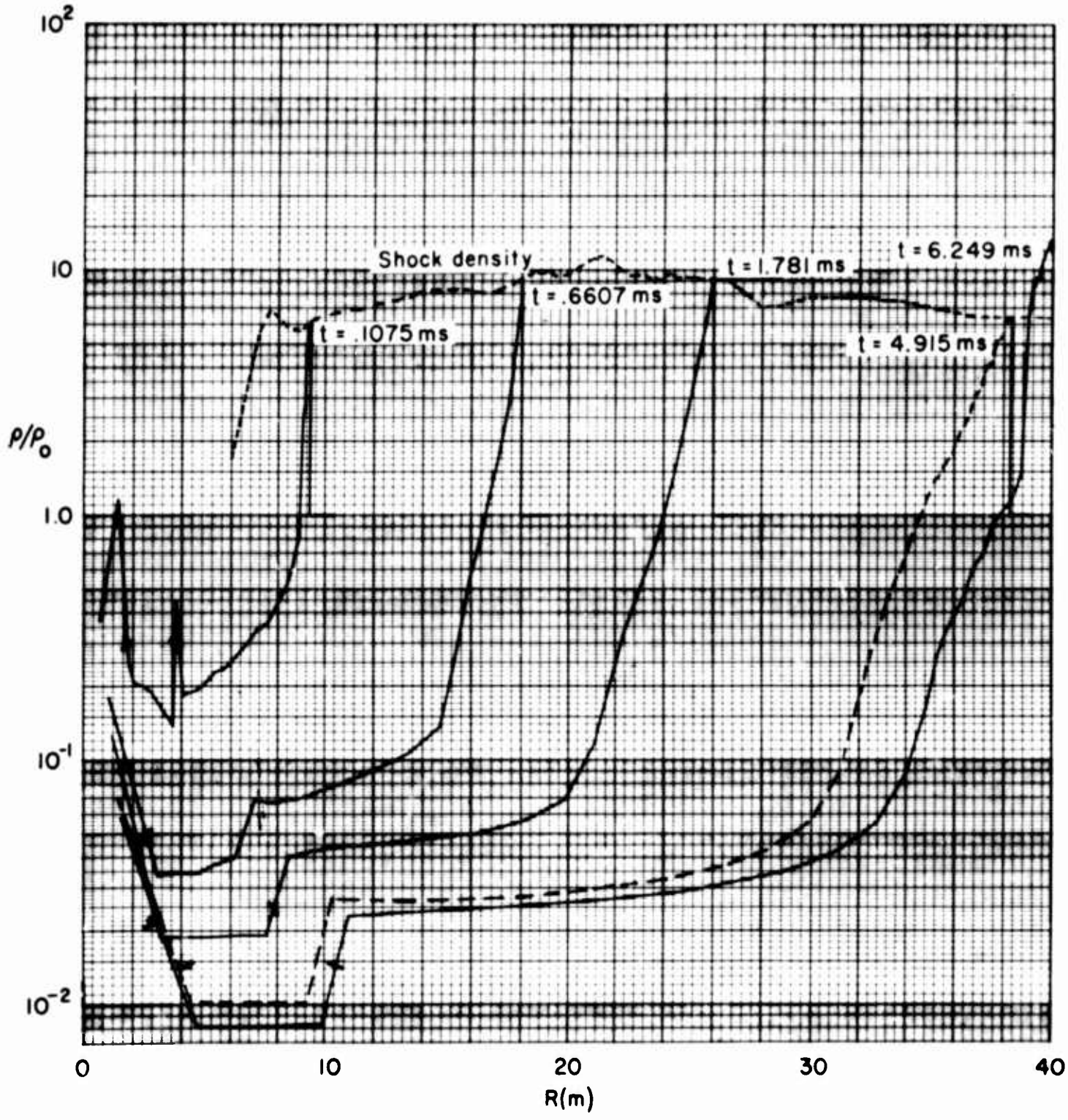

Fig. 22—Density profiles before first reflection, $\rho_i = \rho_0$

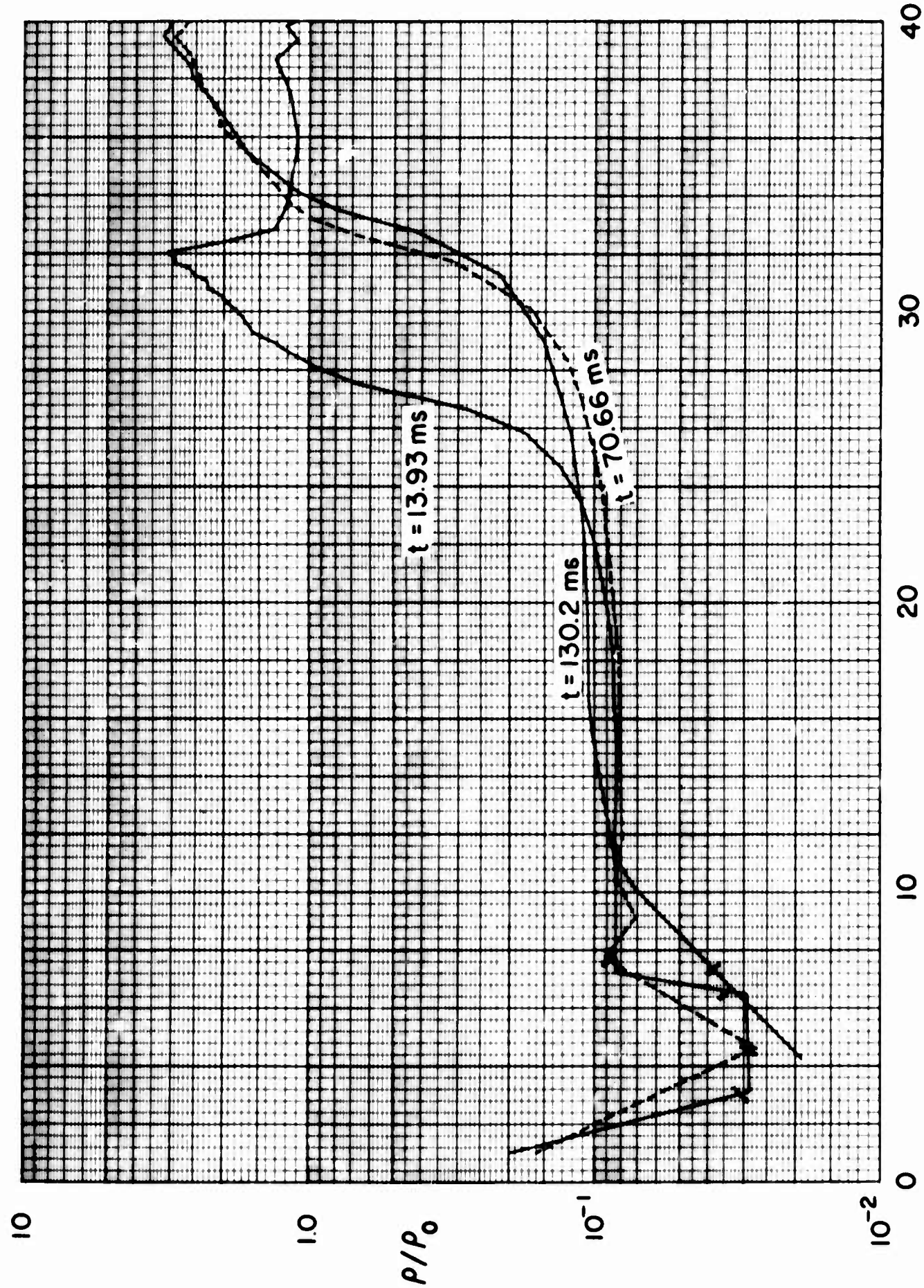

Fig. 23—Late density profiles, $\rho_i = \rho_0$

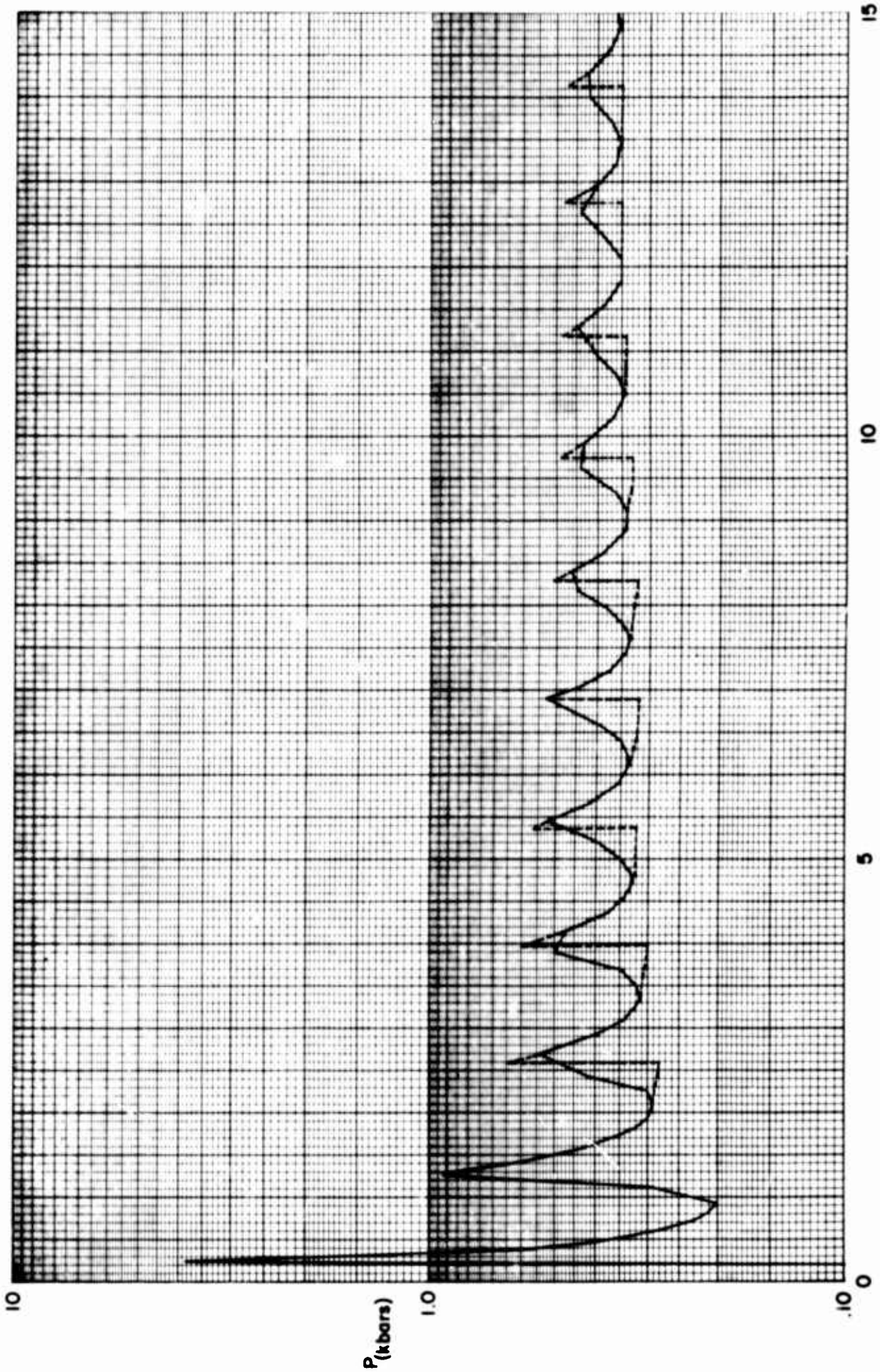

Fig. 24 — Wall pressure versus time, 20 m cavity, $\rho_i = \rho_0/10$

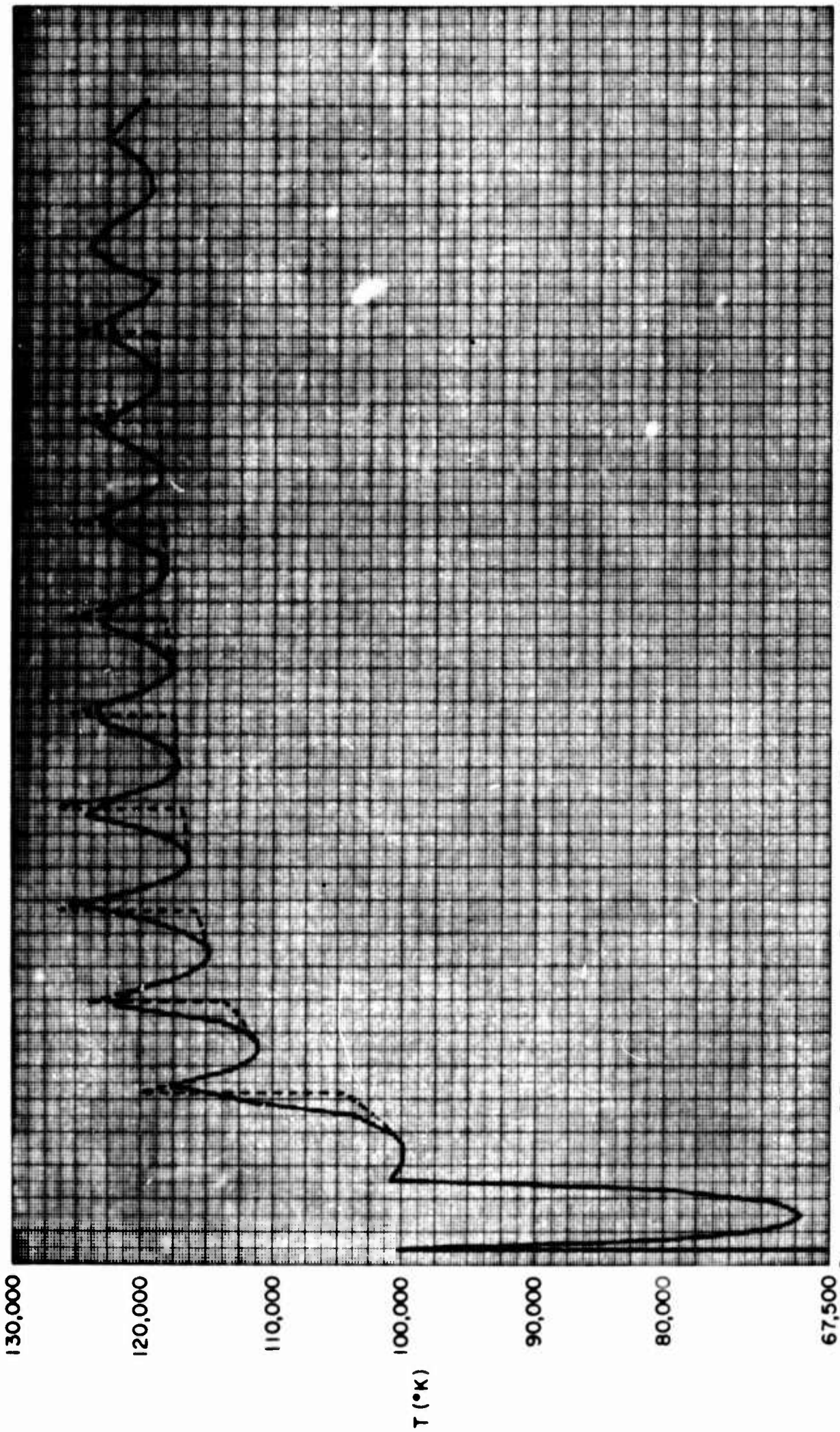

Fig. 25—Wall temperature versus time, 20 m cavity, $\rho_i = \rho_0 / 10$

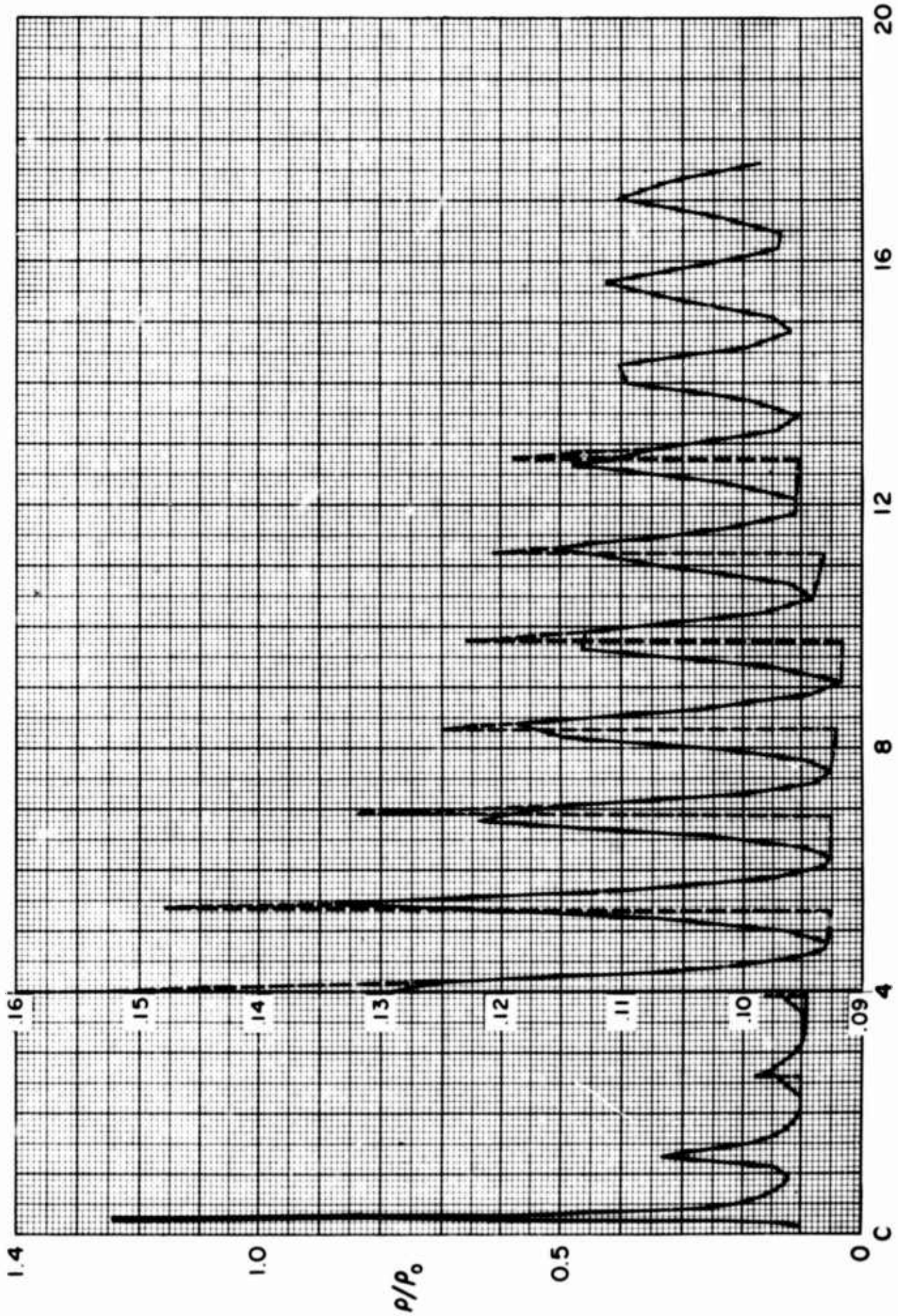

Fig. 26—Wall density ratio versus time, 20 m cavity, $\rho_i = \rho_o/10$

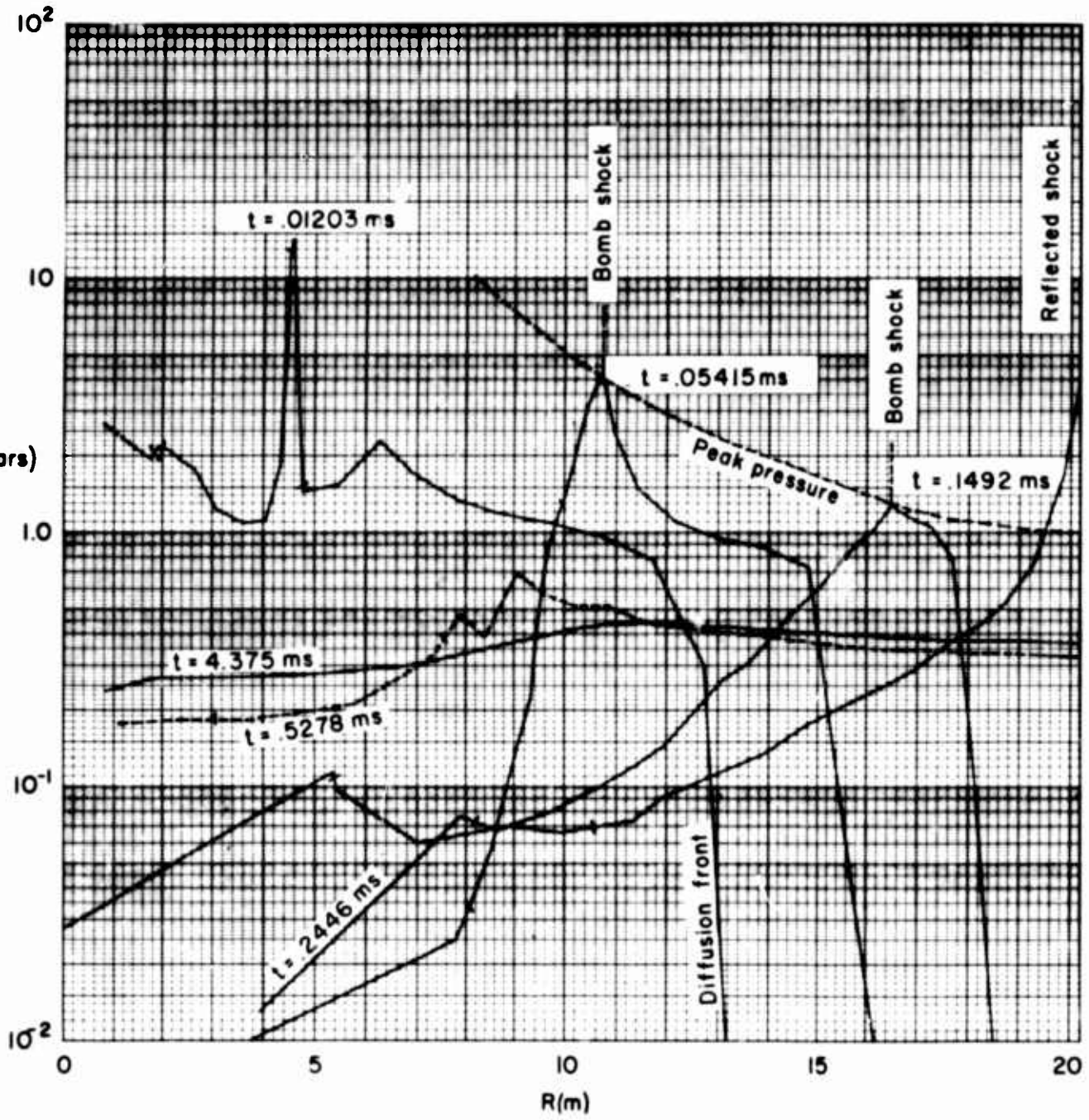

Fig. 27—Pressure profiles, 20 m cavity, $\rho_i = \rho_0 / 10$

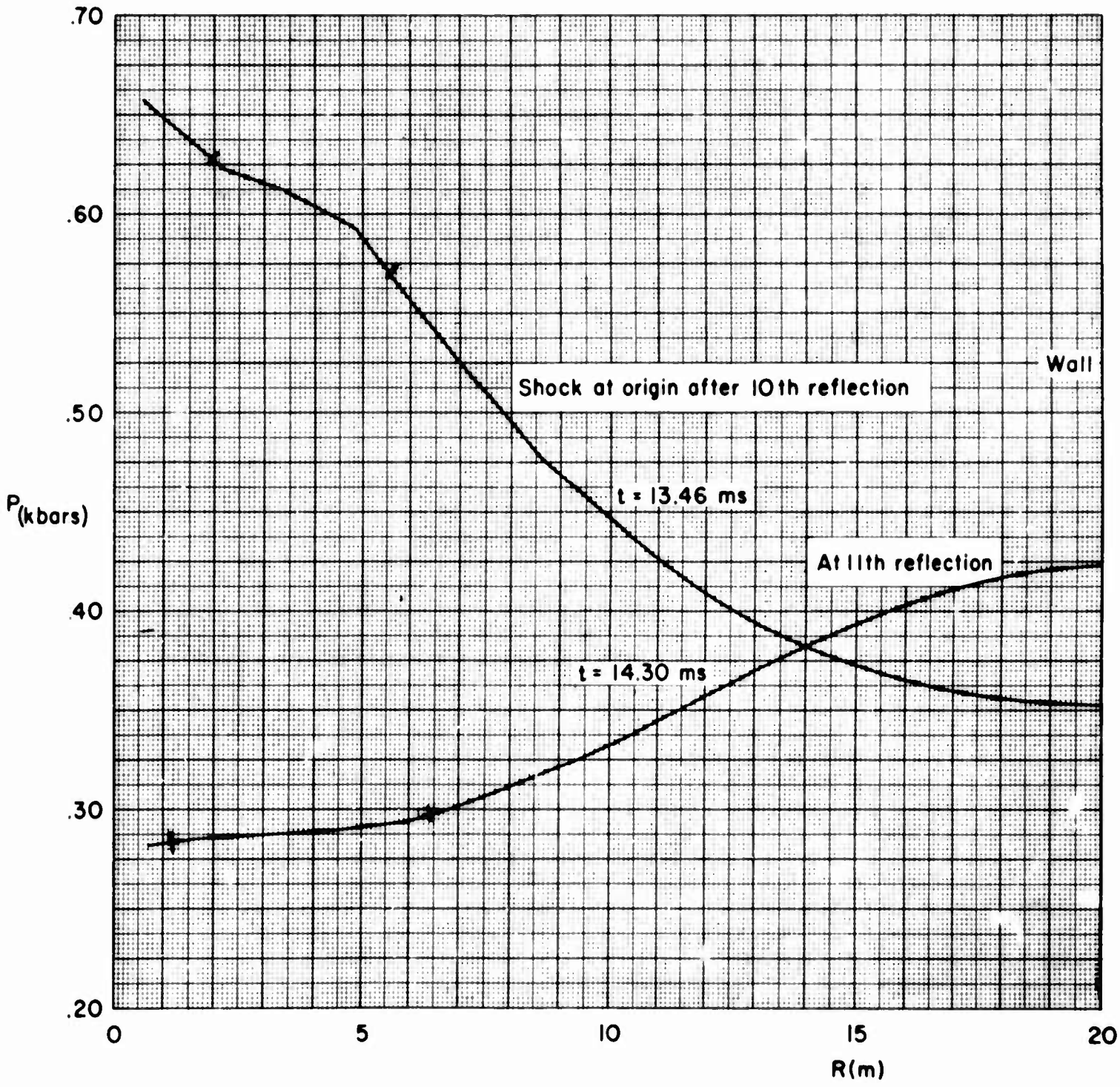

Fig. 28—Late pressure profiles, $\rho_i = \rho_0/10$

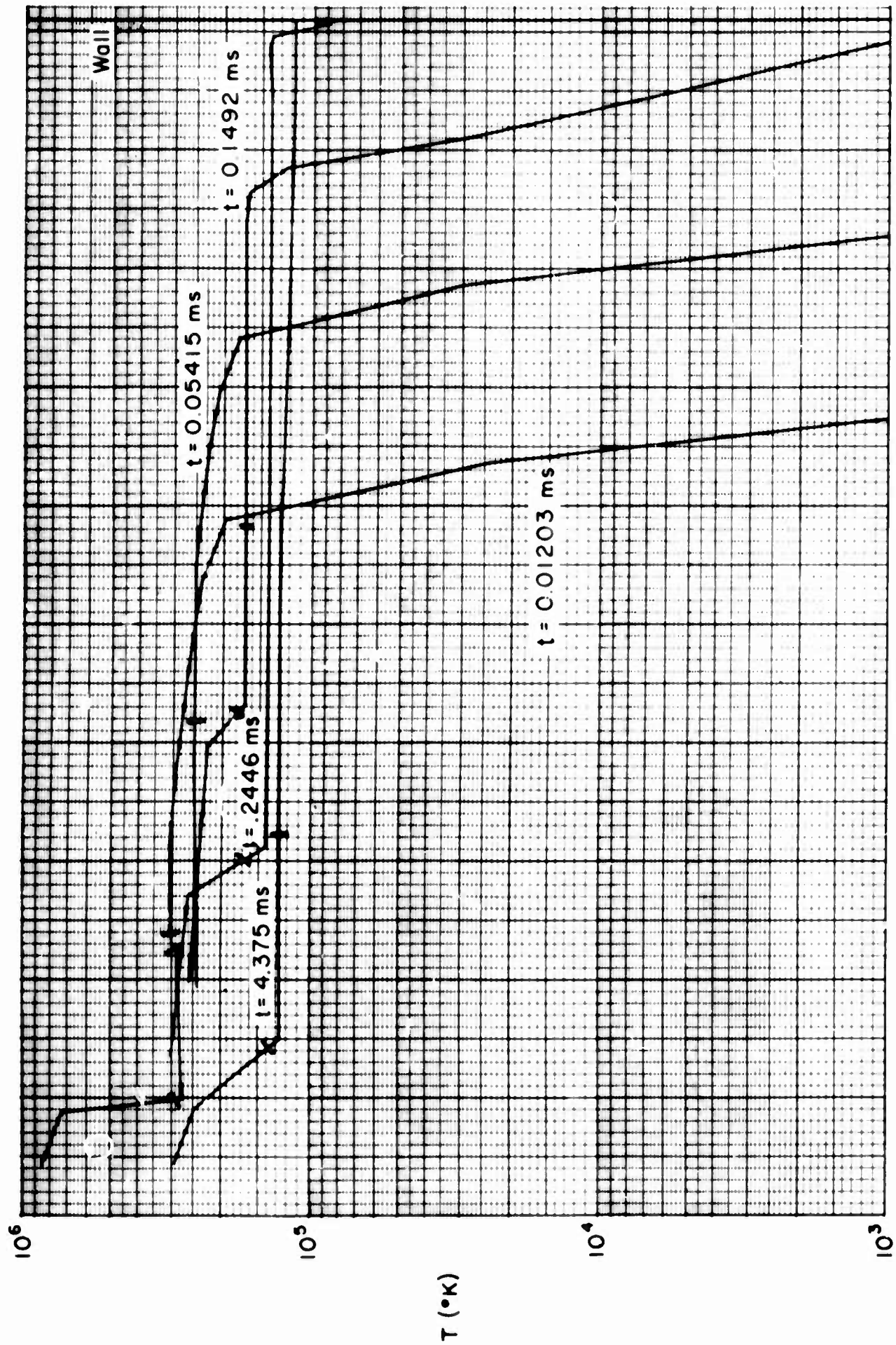

Fig. 29—Early temperature profiles, $\rho_i = \rho_0/10$

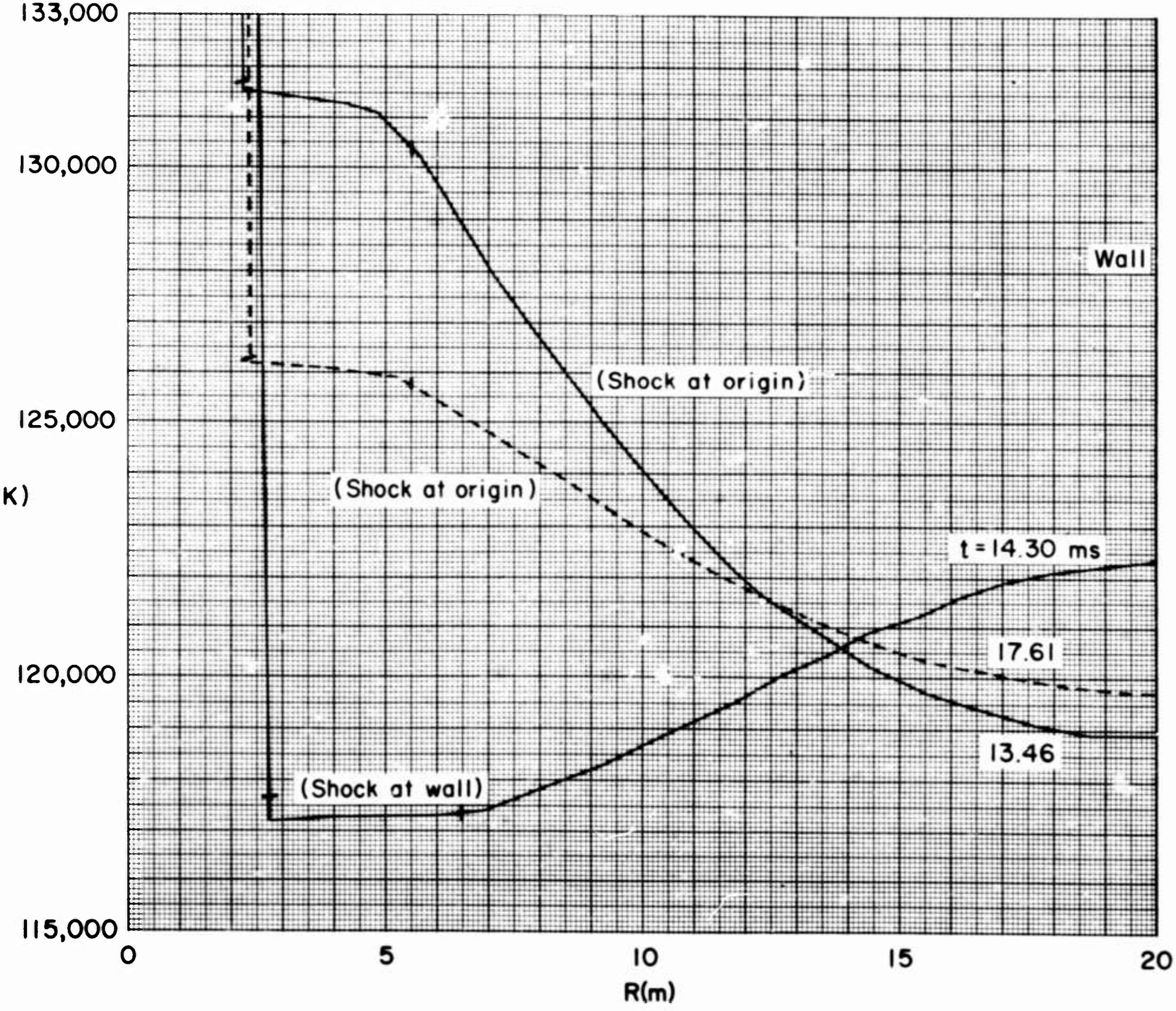

Fig. 20 — Late temperature profiles, $\beta = \beta_c/10$

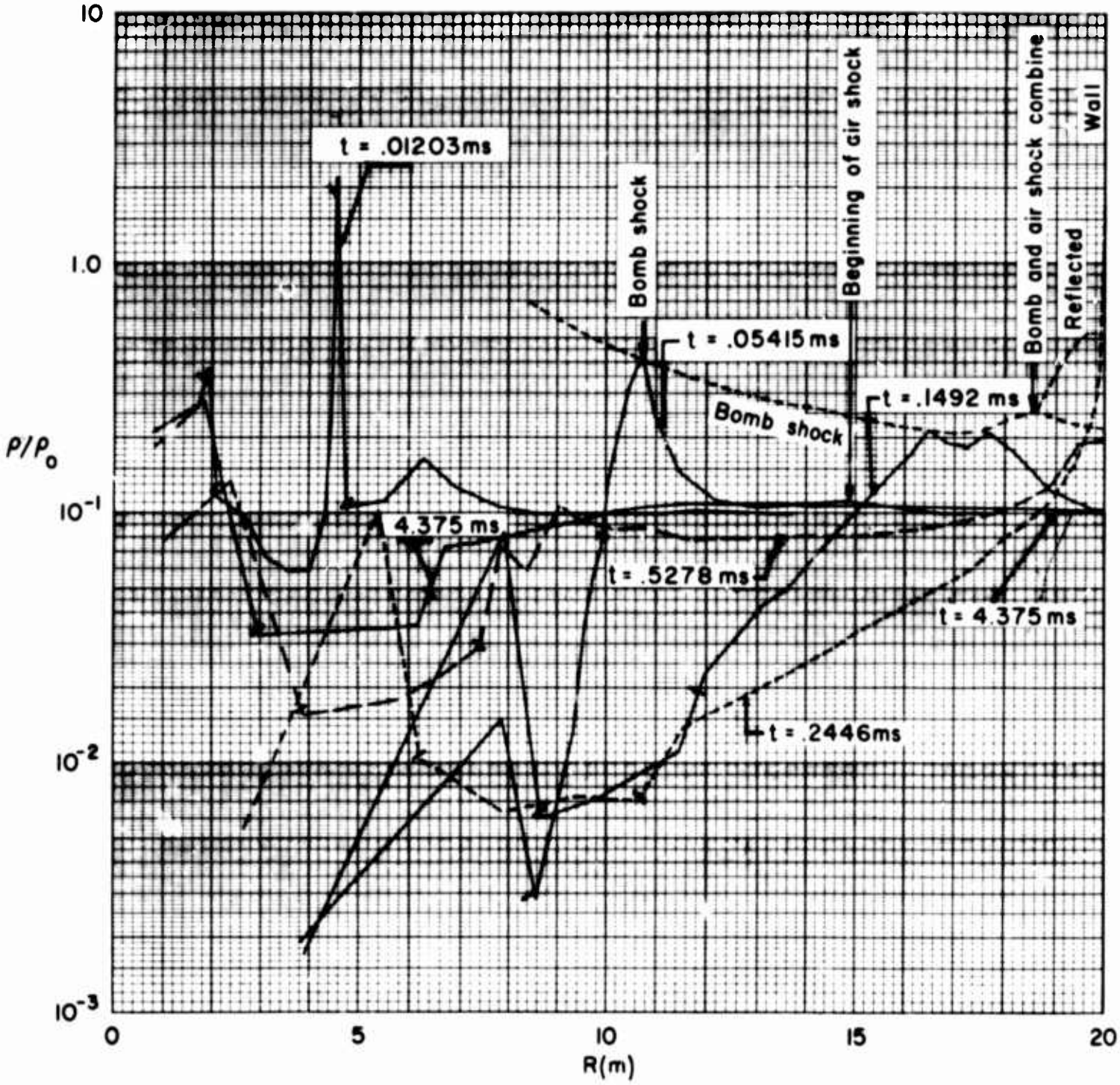

Fig. 31—Early density ratio profiles $\rho_i = \rho_0/10$

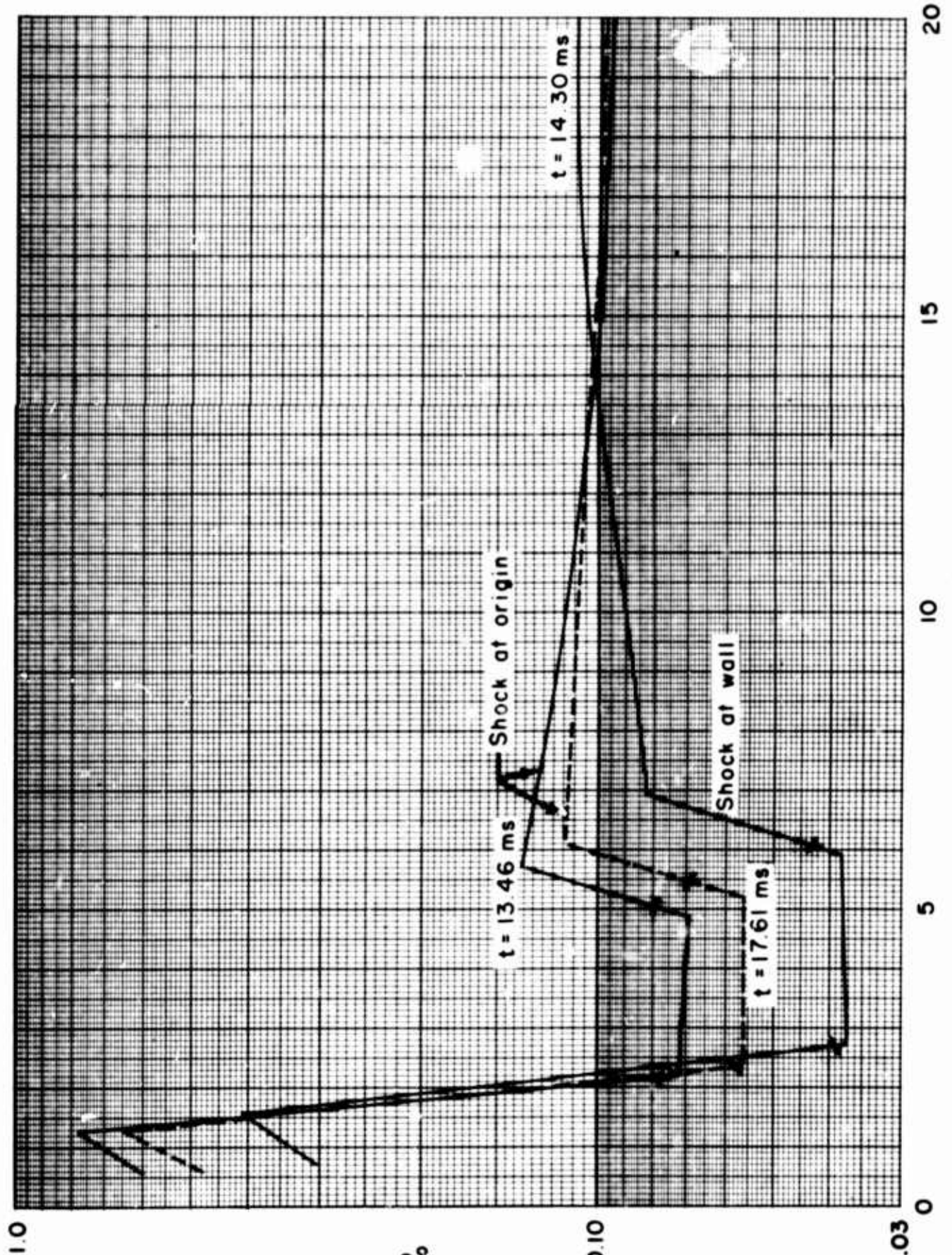

Fig. 32—Late density ratio profiles, $\rho_i = \rho_0/10$

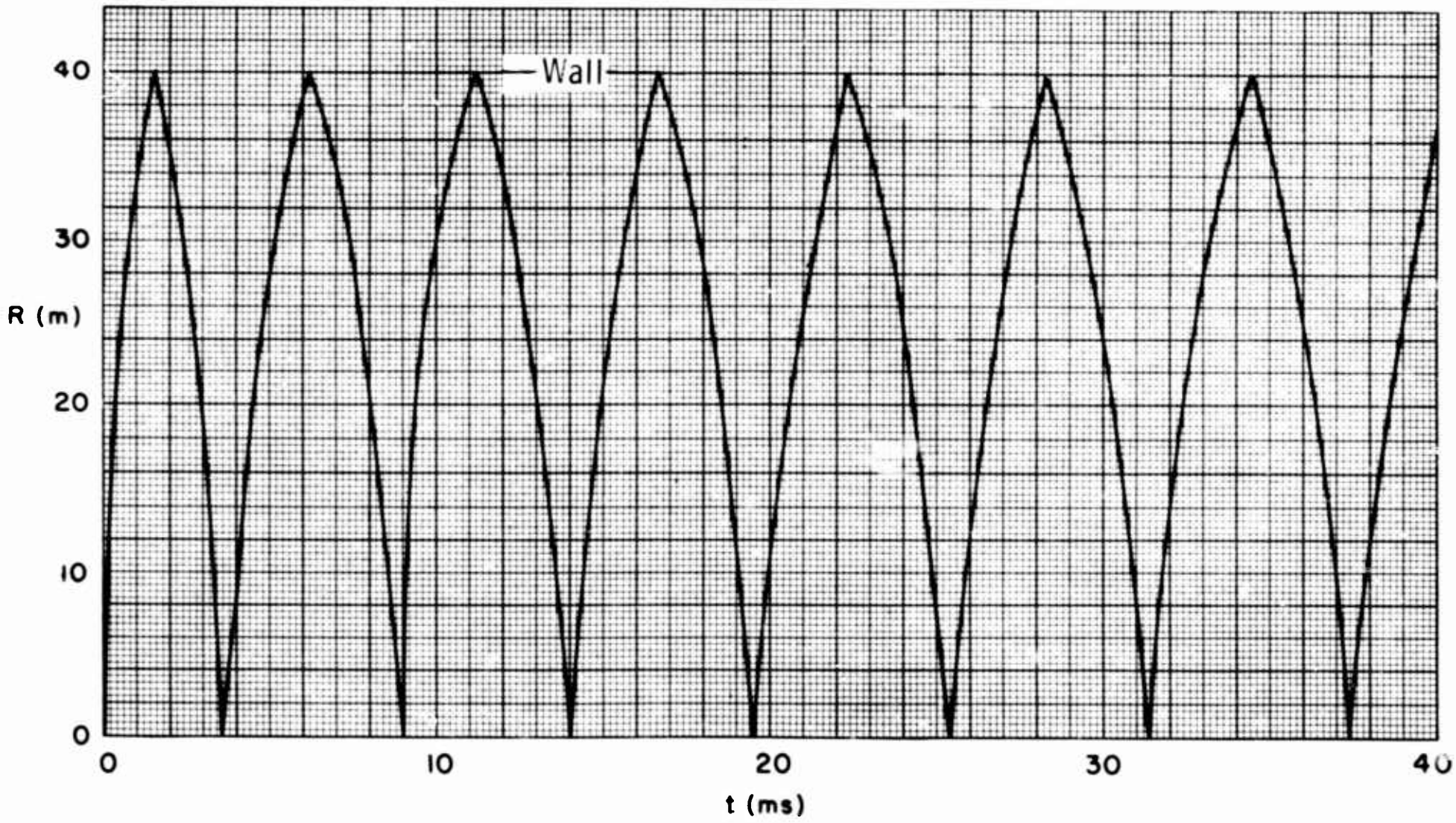

Fig. 33—Shock radius versus time, $P_i = P_0/10$

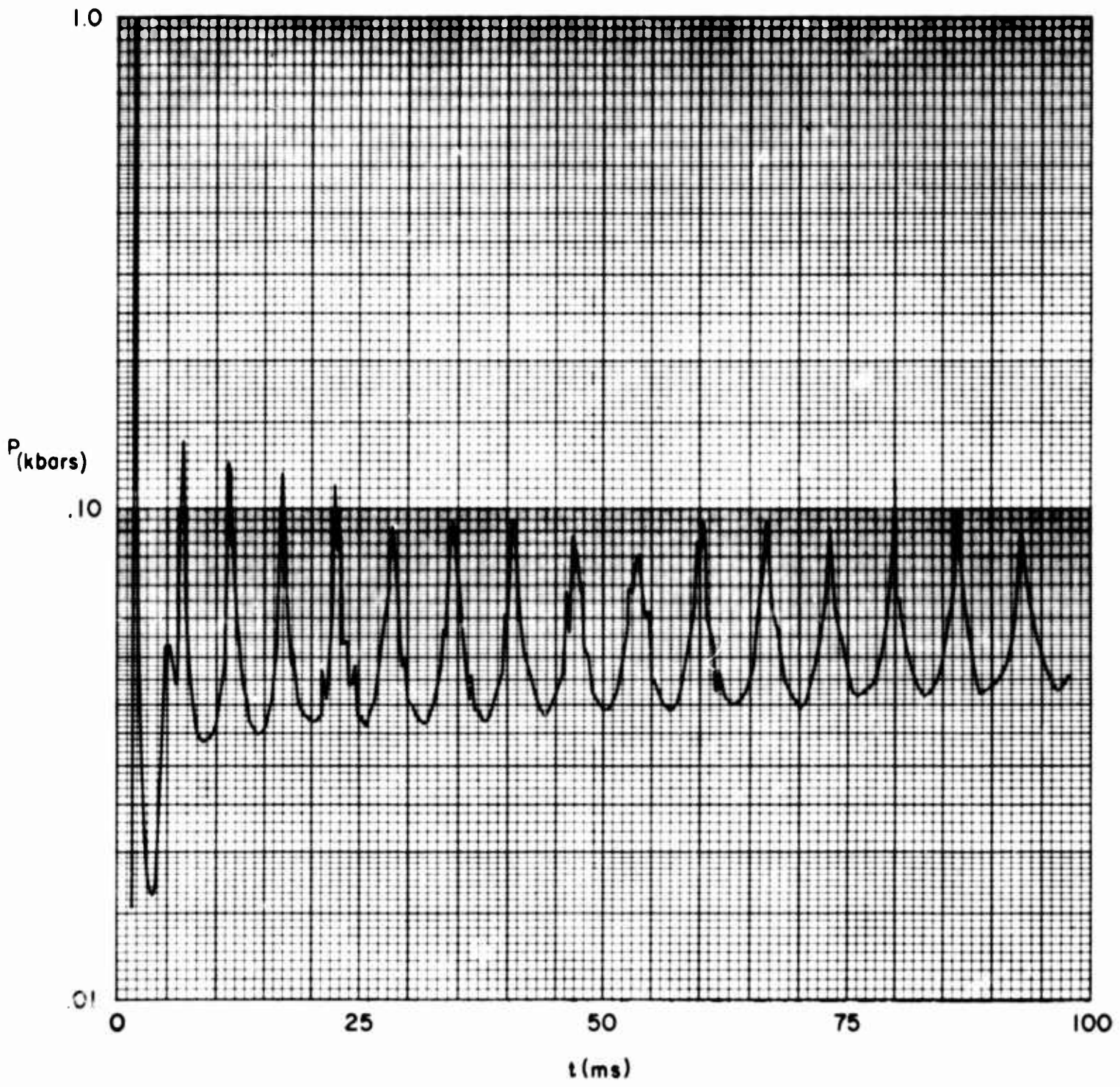

Fig. 34—Wall pressure versus time, 40 m cavity, $P_i = P_0/10$

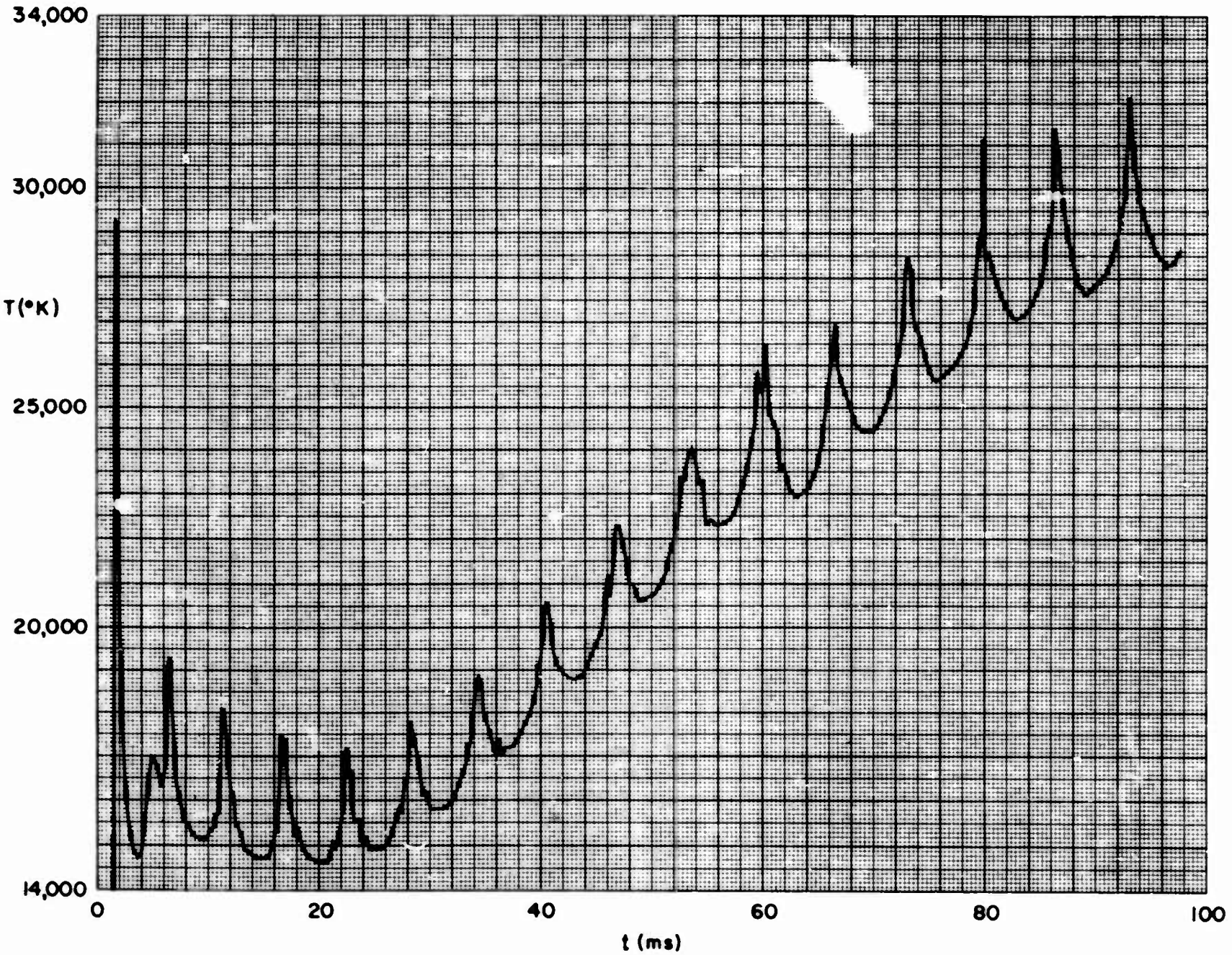

Fig. 35—Wall temperature versus time, 40 m cavity, $\rho_i = \rho_0 / 10$

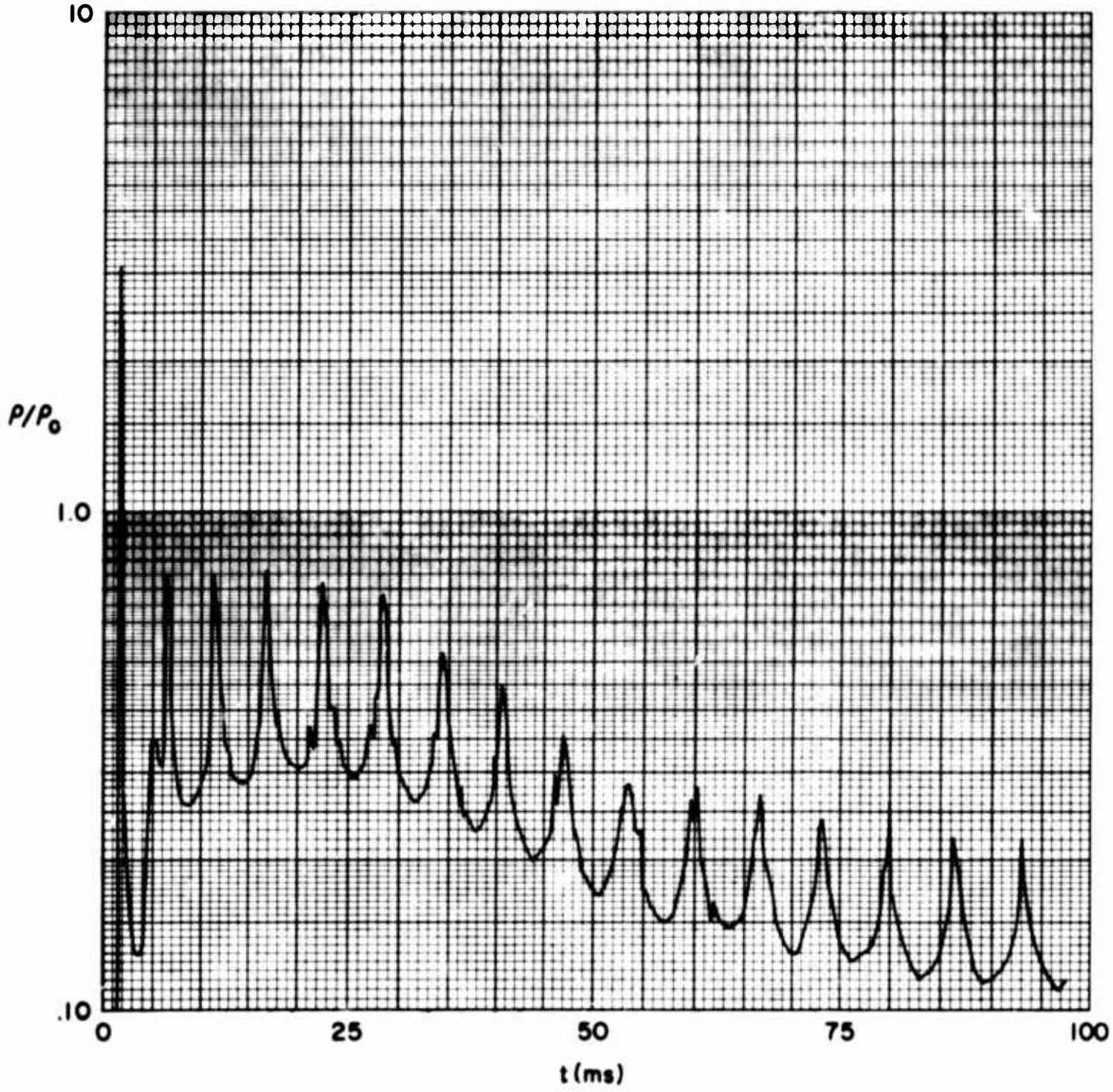

Fig. 36—Wall density ratio versus time, 40 m cavity, $\rho_i = \rho_0 / 10$

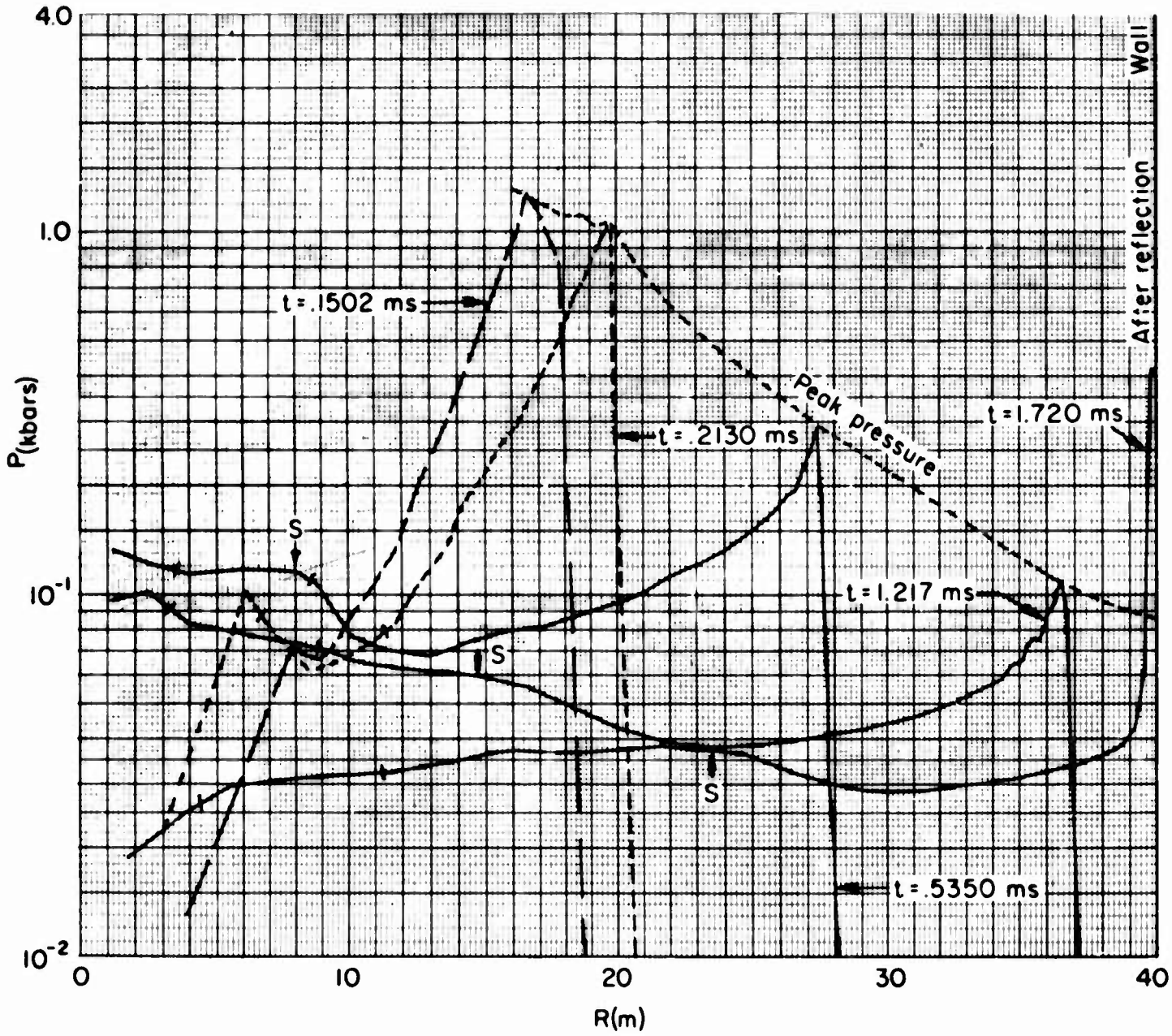

Fig. 37—Pressure versus radius at times up to first reflection $\rho_i = \rho_0/10$

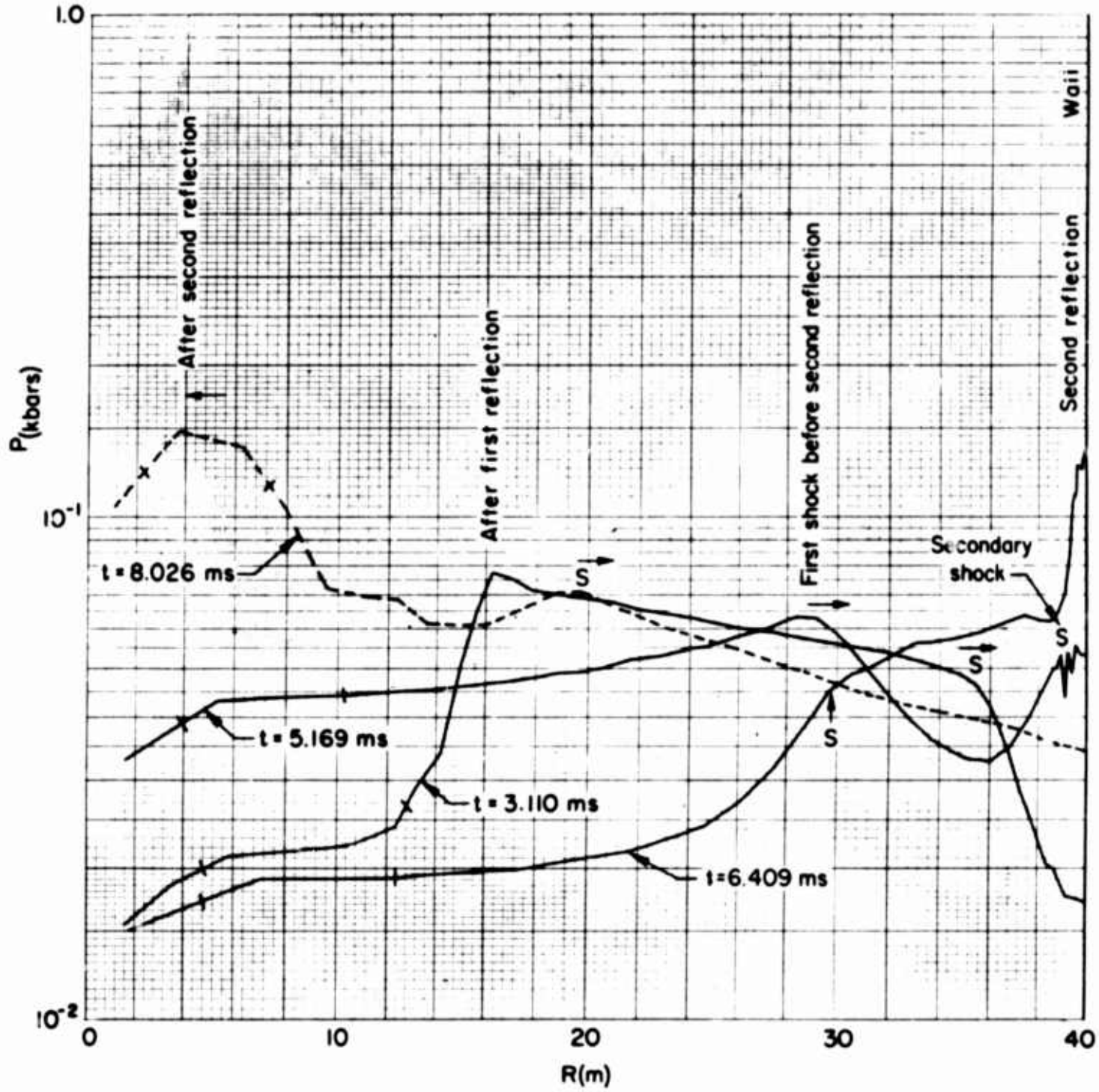

Fig. 38—Pressure versus radius at times between first and third reflections, $\rho_i = \rho_0 / 10$

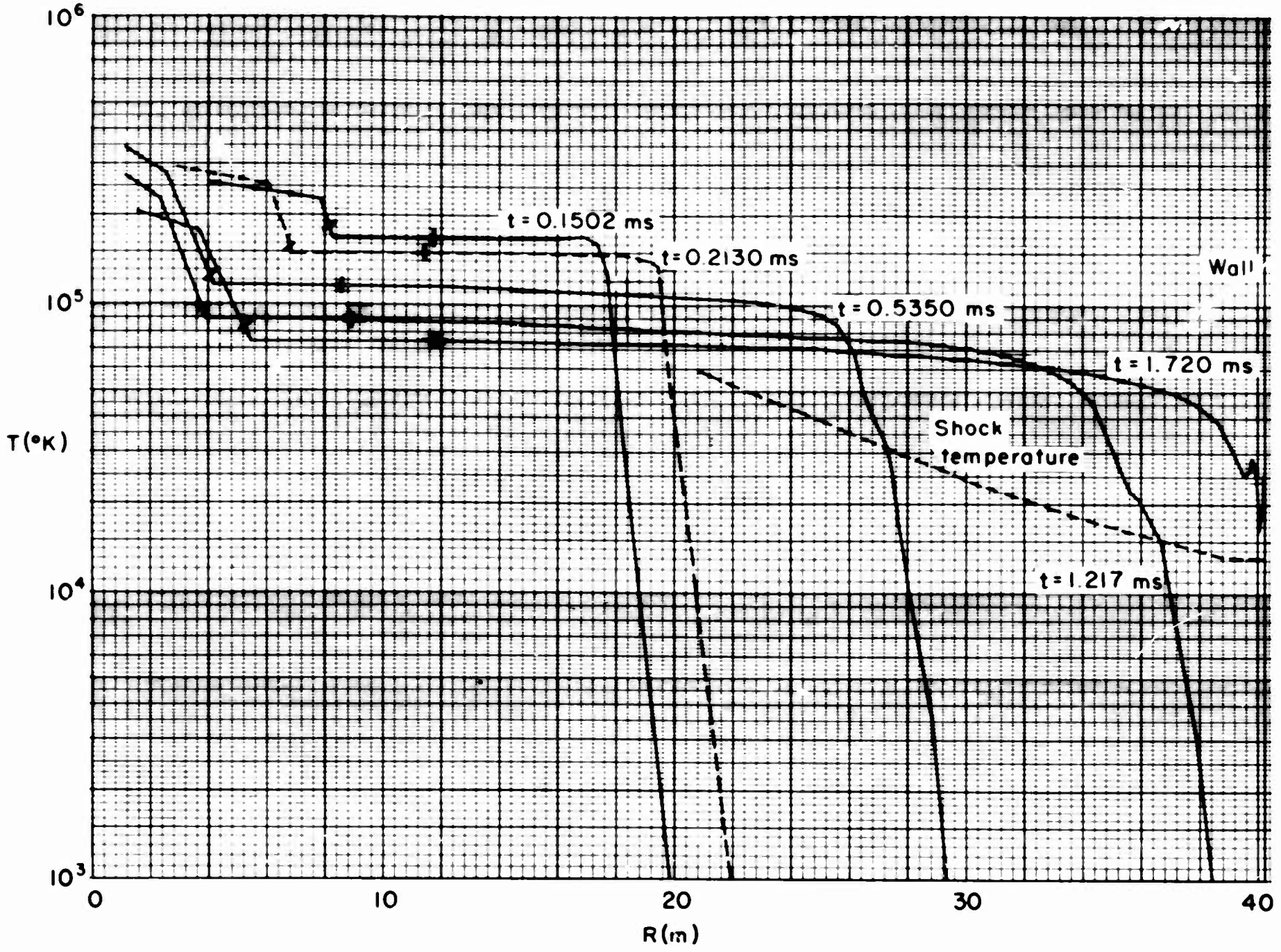

Fig. 39—Temperature profiles at early times (before first reflection), $\rho_i = \rho_0/10$

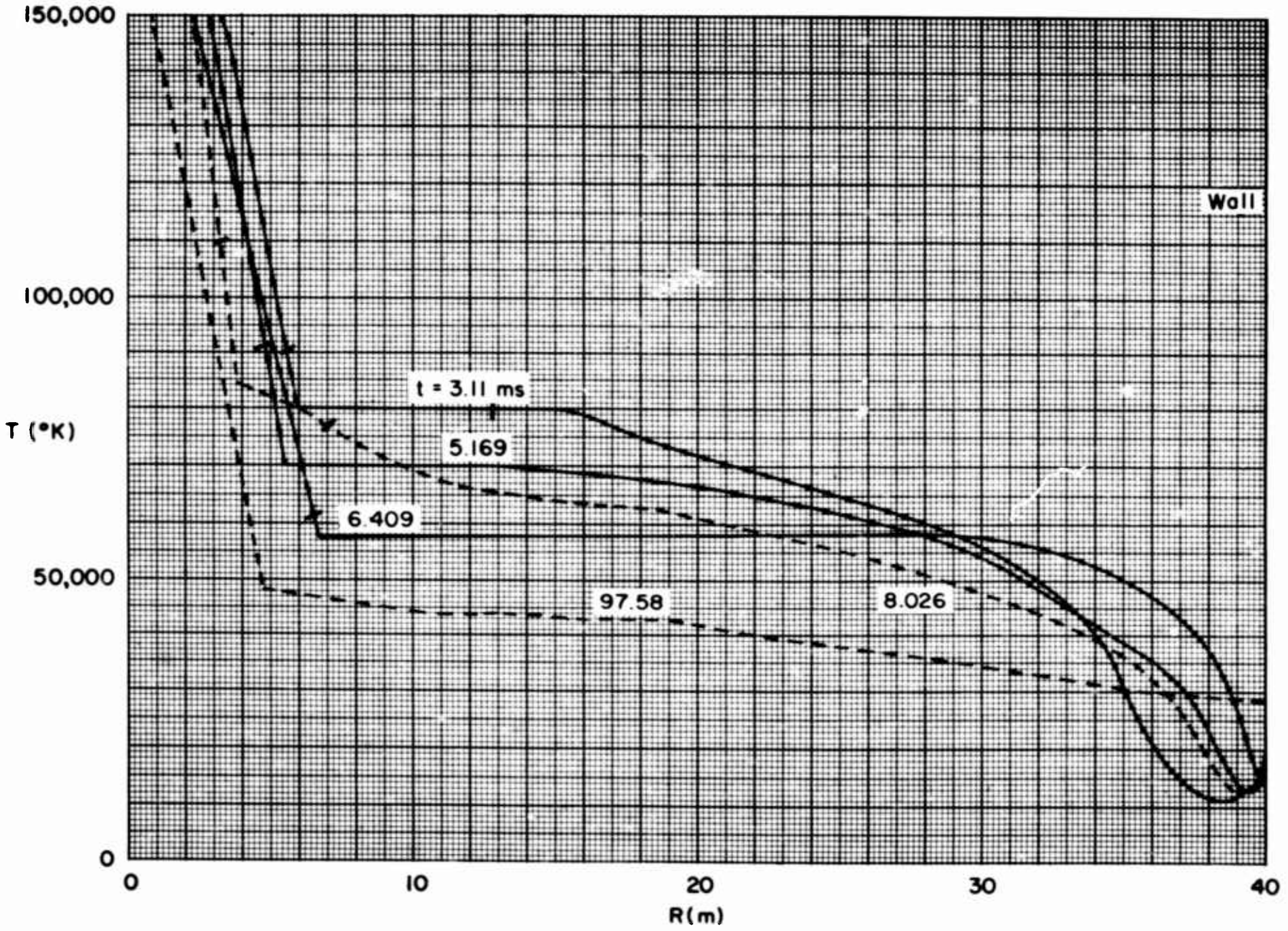

Fig. 40—Late temperature profiles, $\rho_i = \rho_0/10$

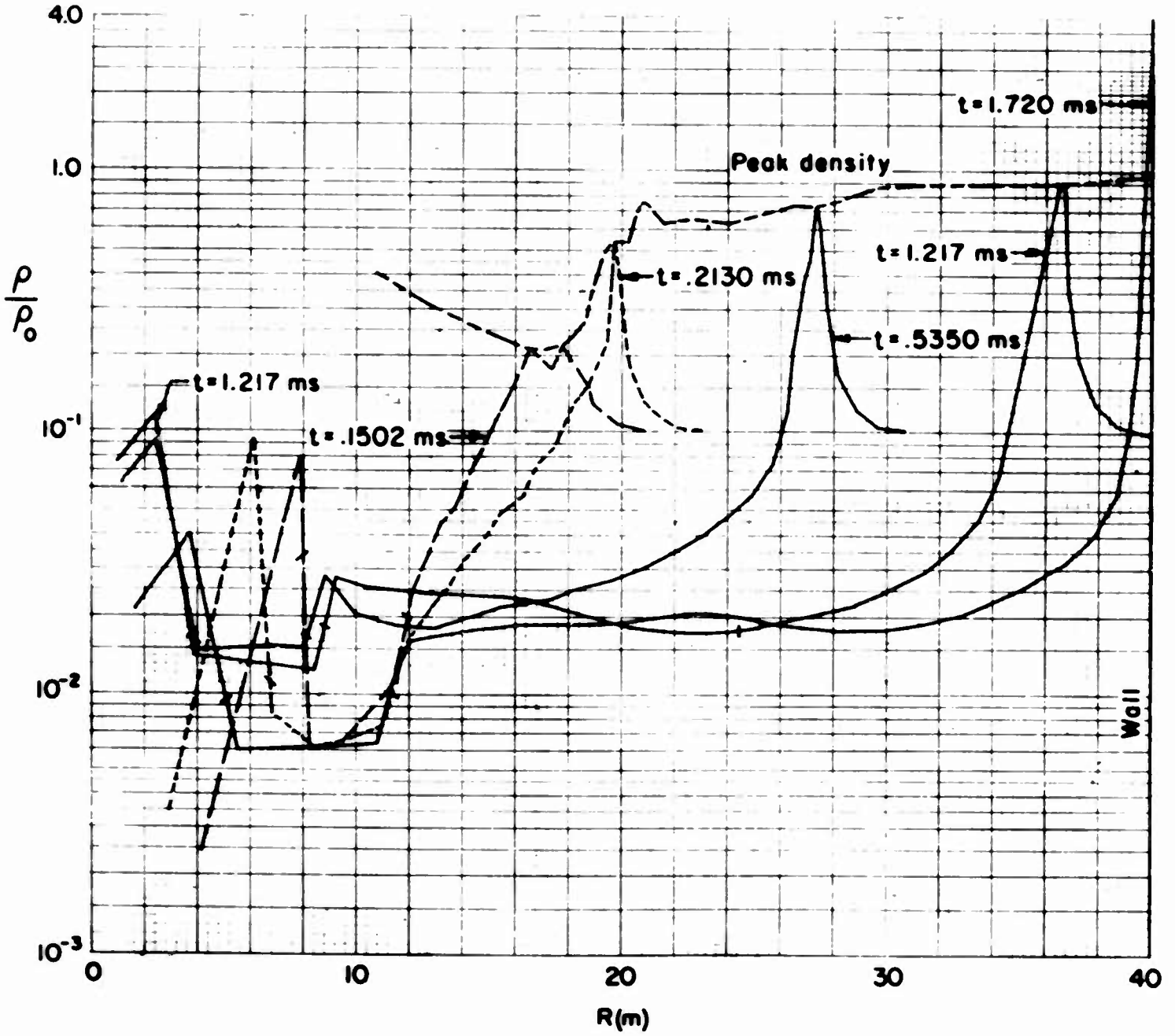

Fig. 41 — Density versus radius at times up to first reflection, $\rho_1 = \rho_0 / 10$

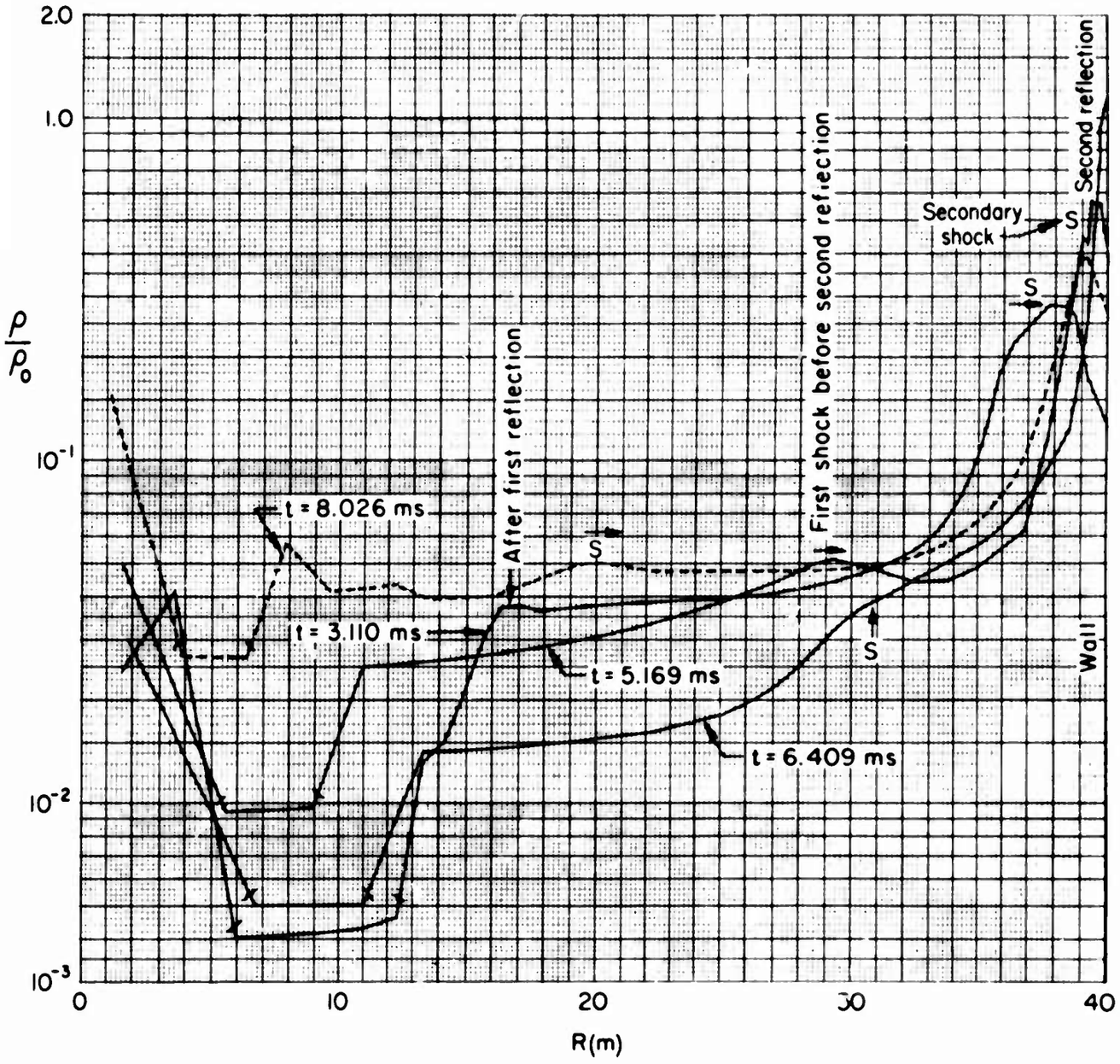

Fig. 42—Density versus radius at times between first and third reflections, $\rho_i = \rho_0/10$

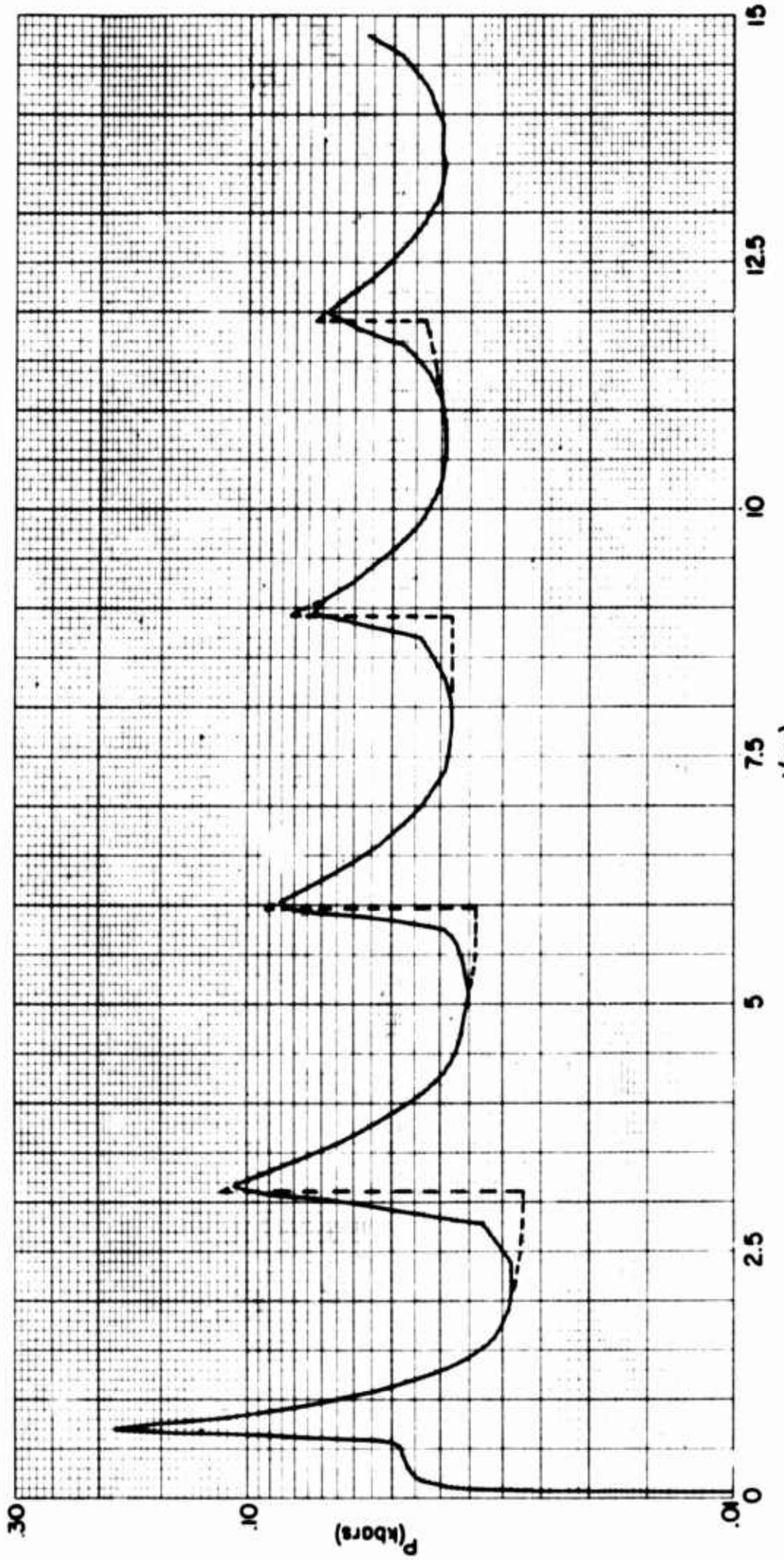

Fig. 43—Wall pressure versus time, 40 m cavity, $P_i = P_o/100$

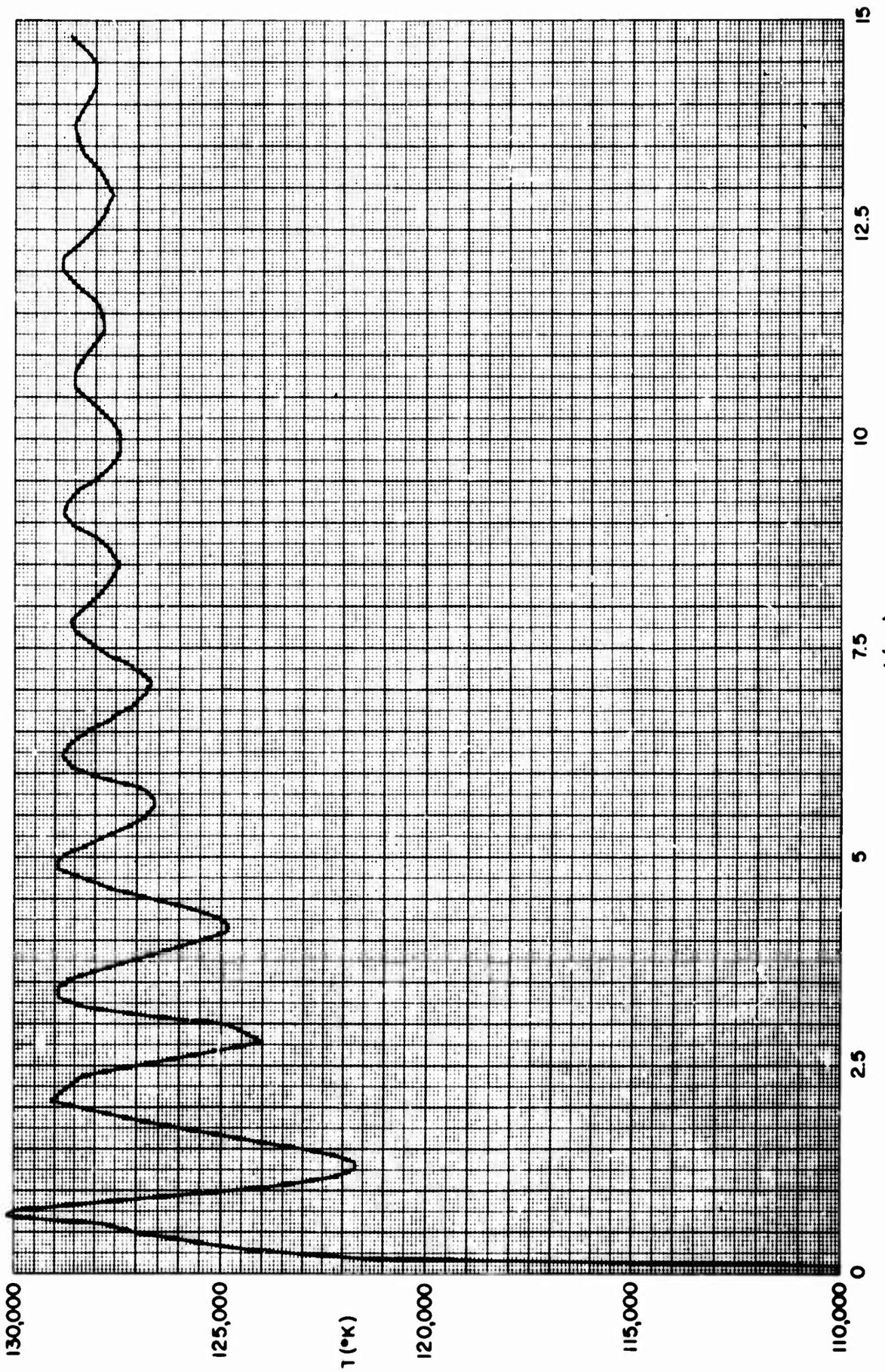

Fig. 44—Wall temperature versus time, 40 m cavity, $\rho_i = \rho_0/100$

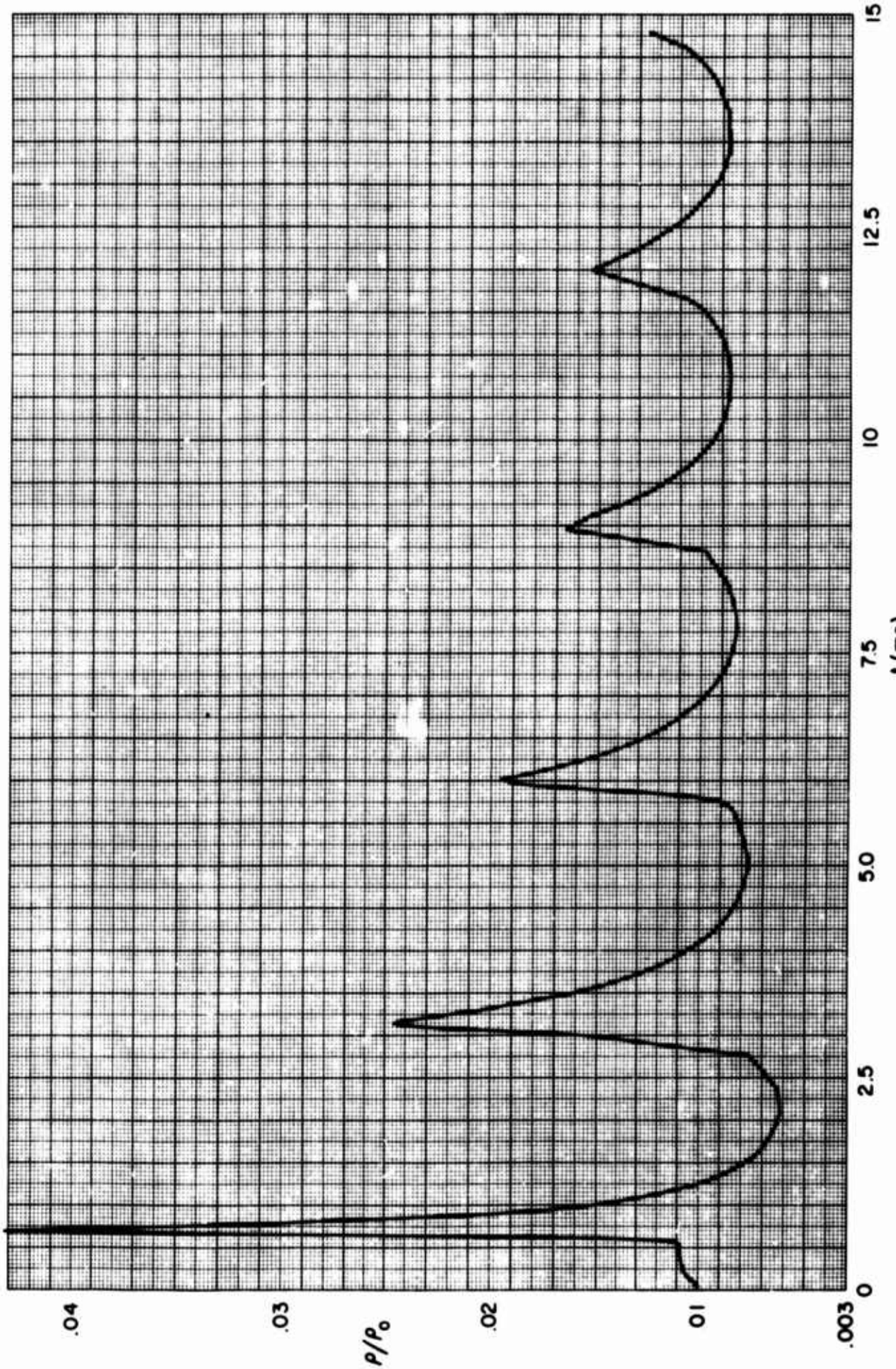

Fig. 45—Wall density ratio versus time, 40 m cavity, $\rho_i = \rho_0/100$

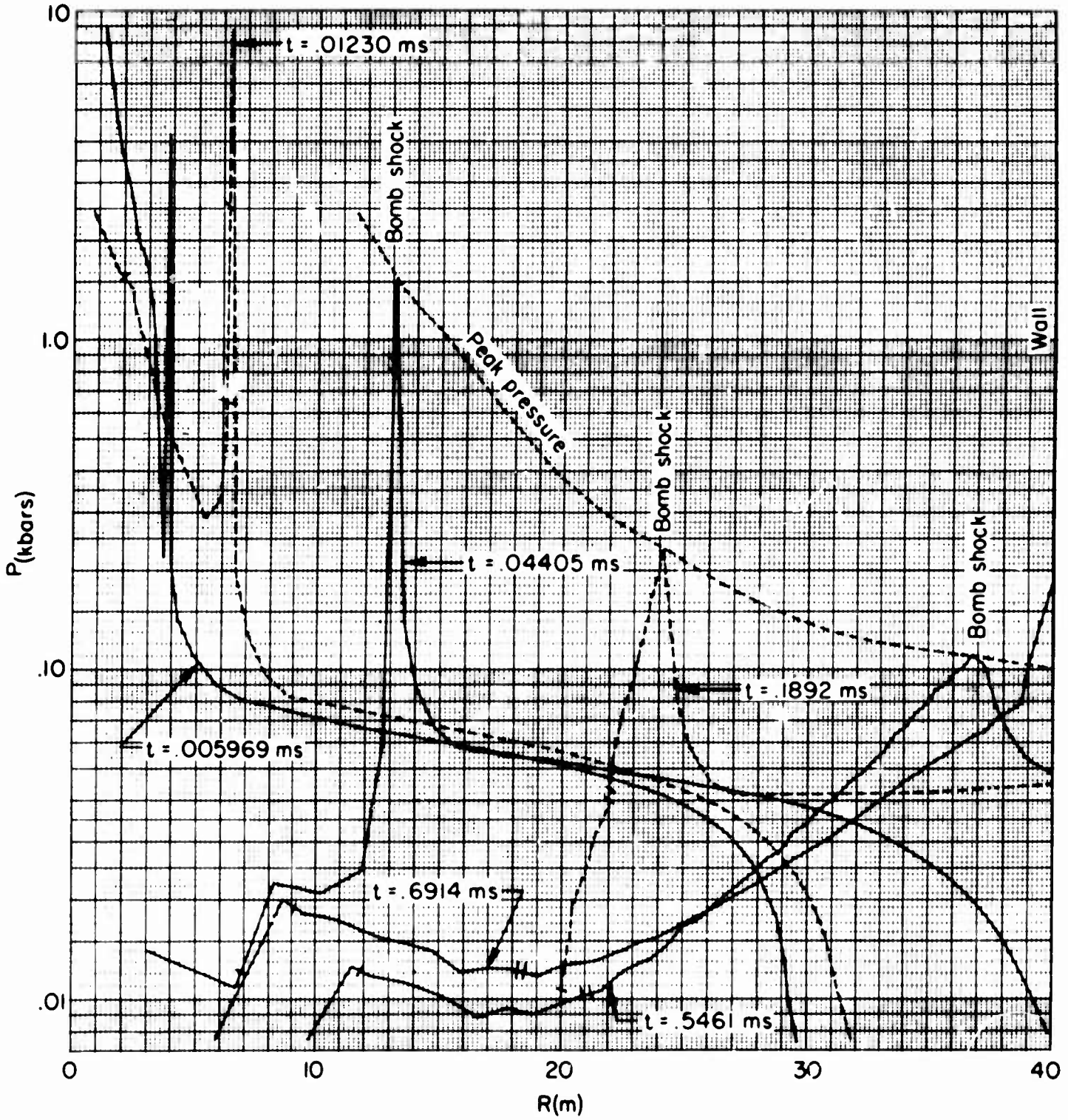

Fig. 46—Pressure versus radius at times before first reflection, 40 m cavity, $\rho_i = \rho_0 / 100$

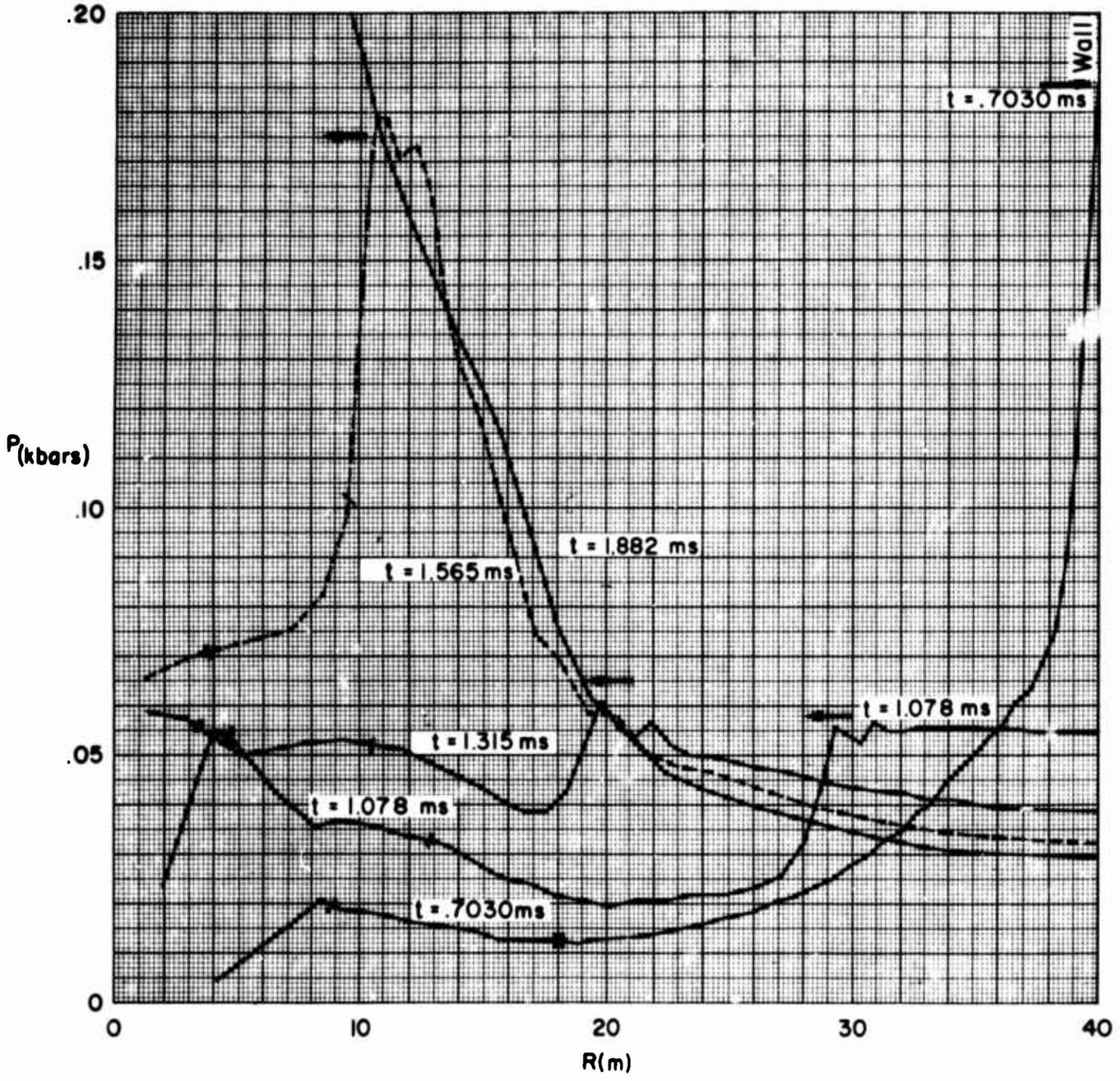

Fig. 47 — Pressure profiles, $\rho_i = \rho_0 / 100$

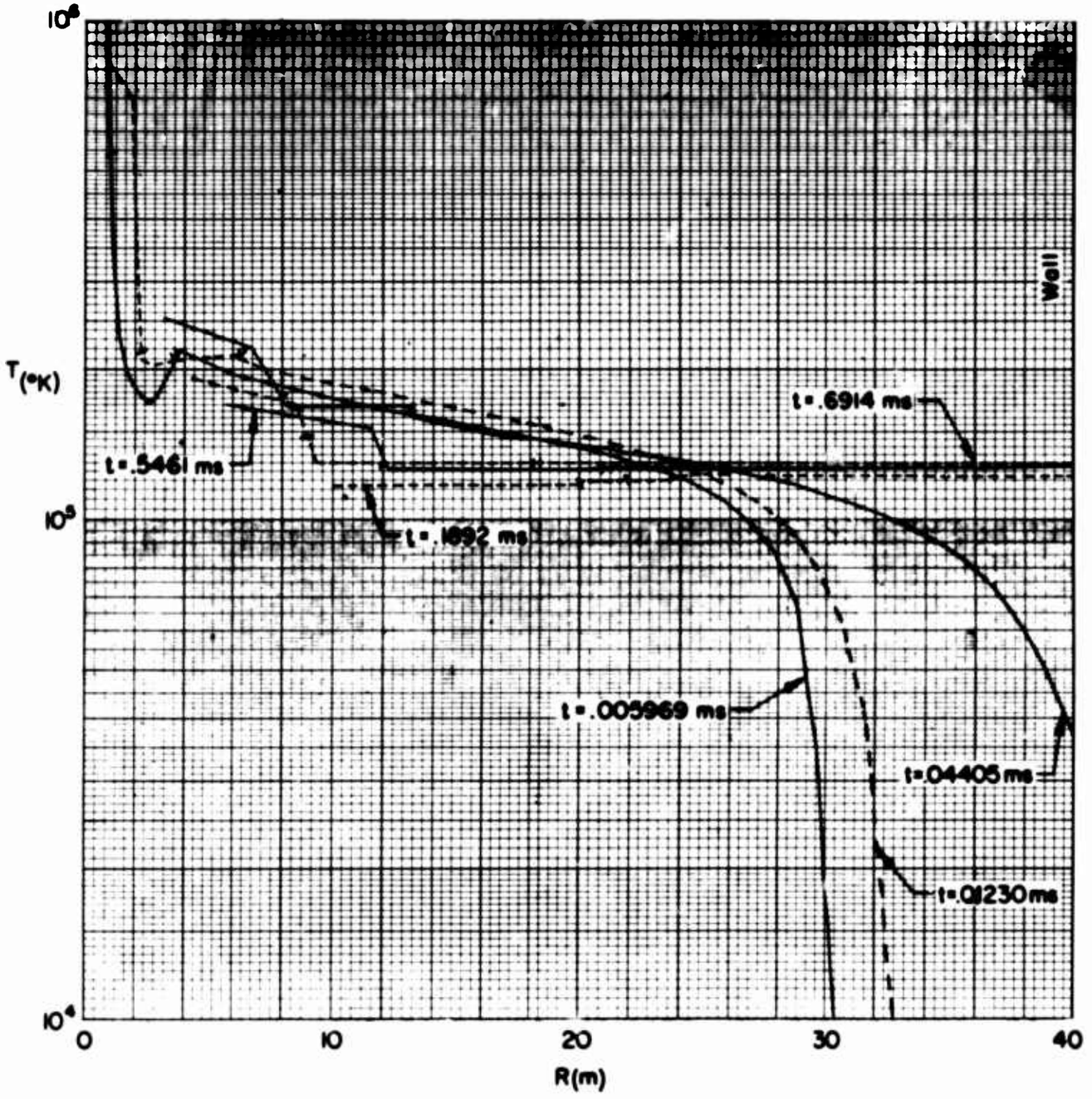

Fig. 48—Temperature versus radius at times before first reflection, $\rho_i = \rho_0/100$

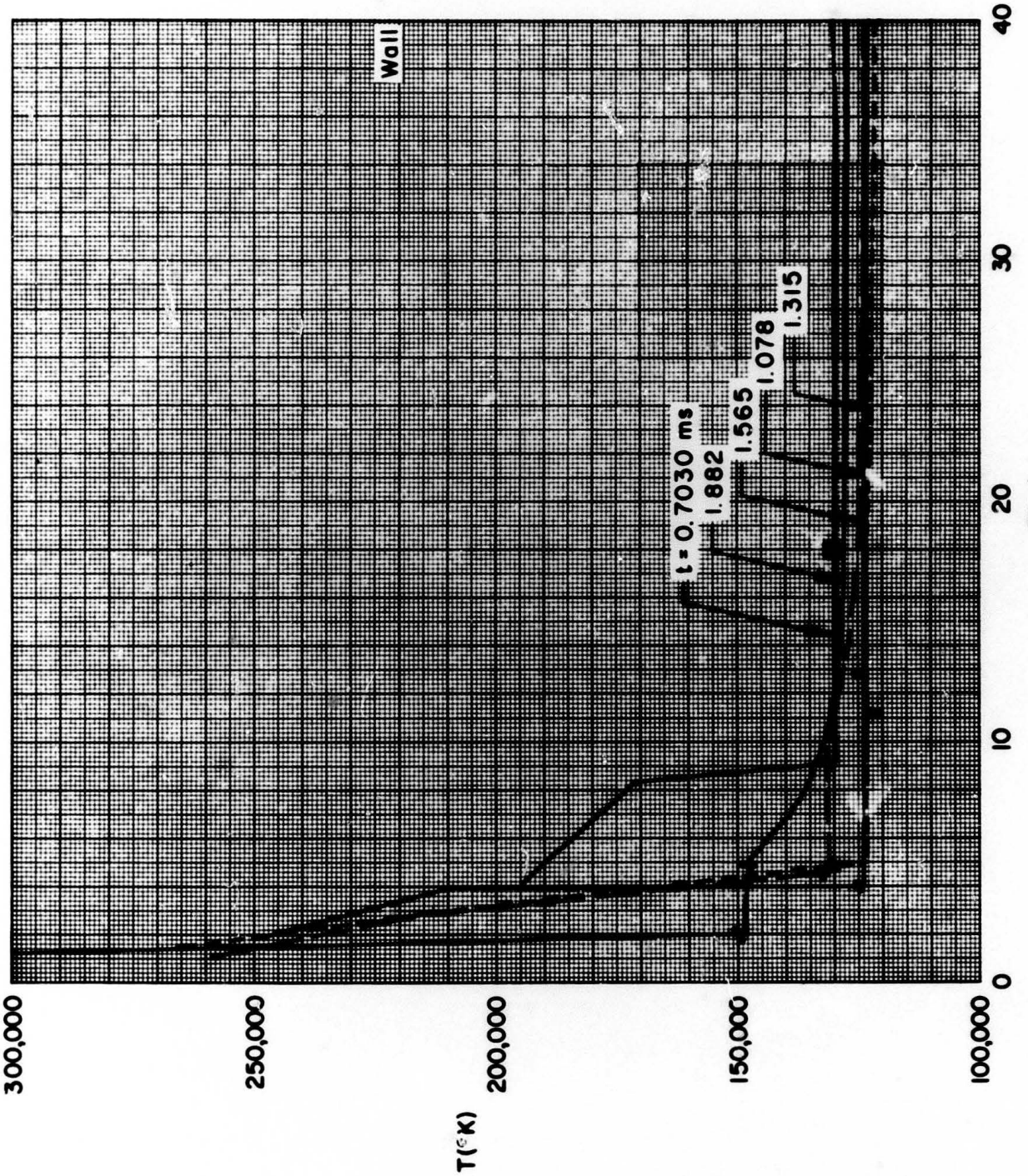

Fig. 49—Temperature profiles, $\rho_i = \rho_0 / 100$

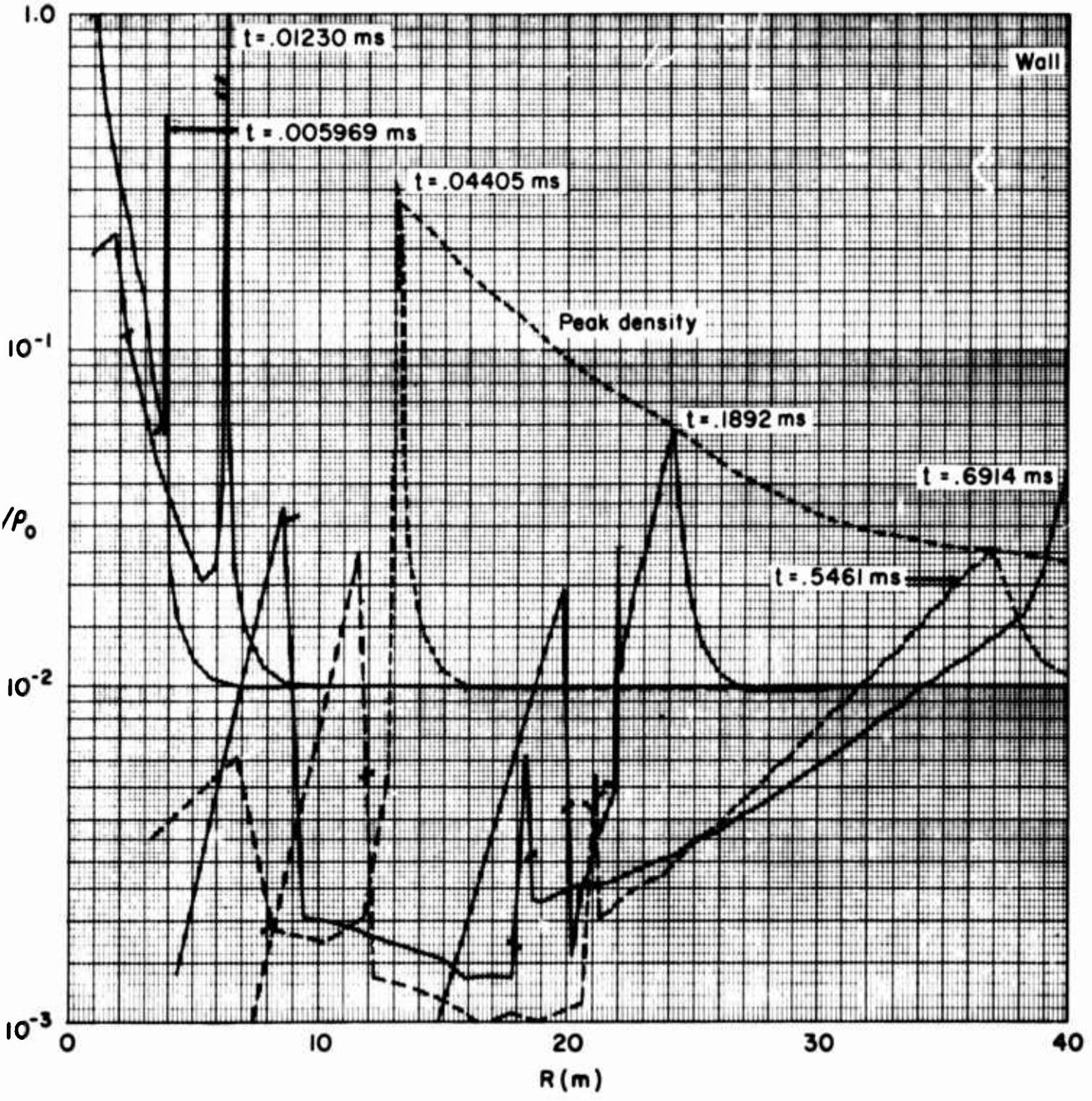

Fig. 50—Early density ratio profiles, $\rho_i = \rho_0 / 100$

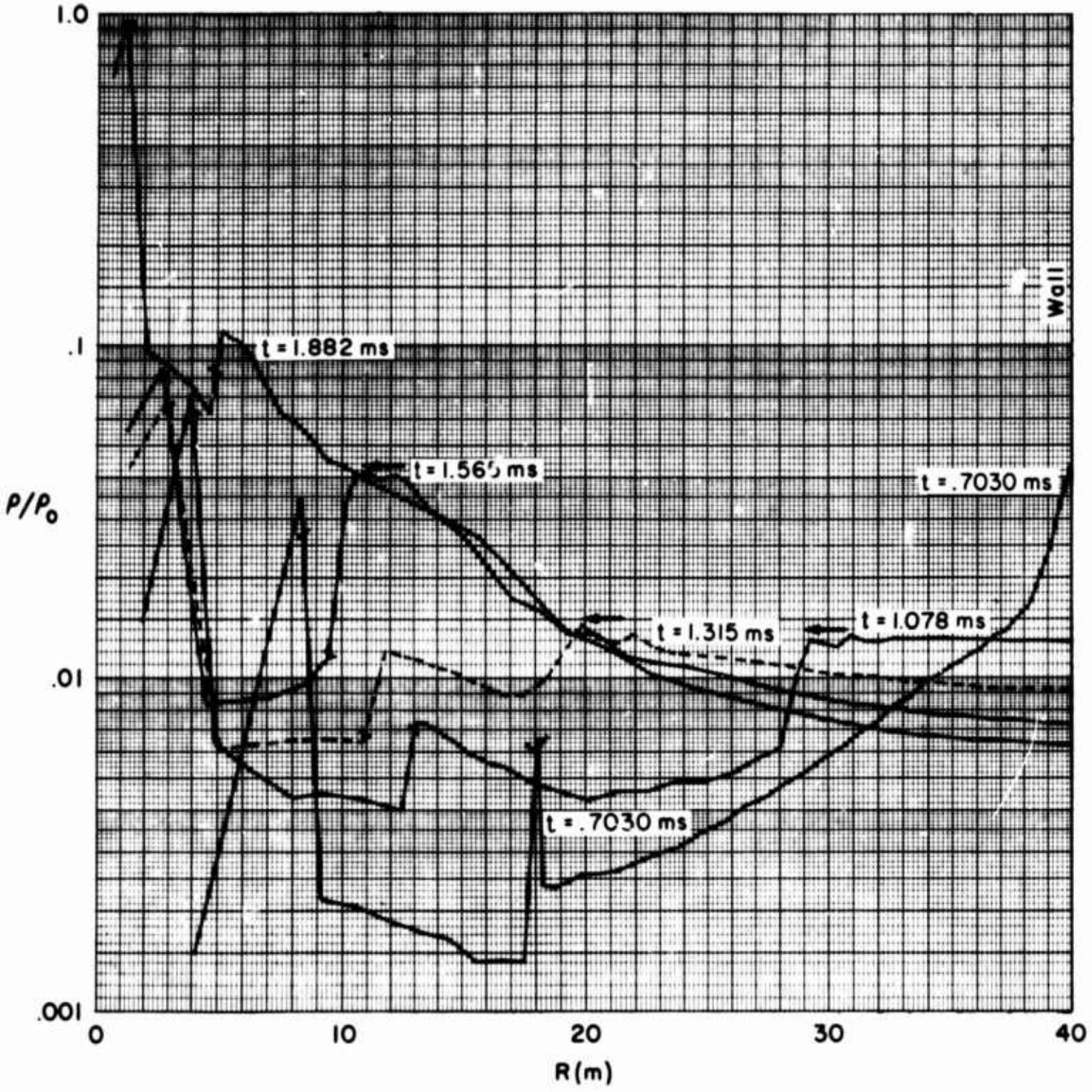

Fig. 51—Late density ratio profiles, $\rho_i = \rho_0 / 100$

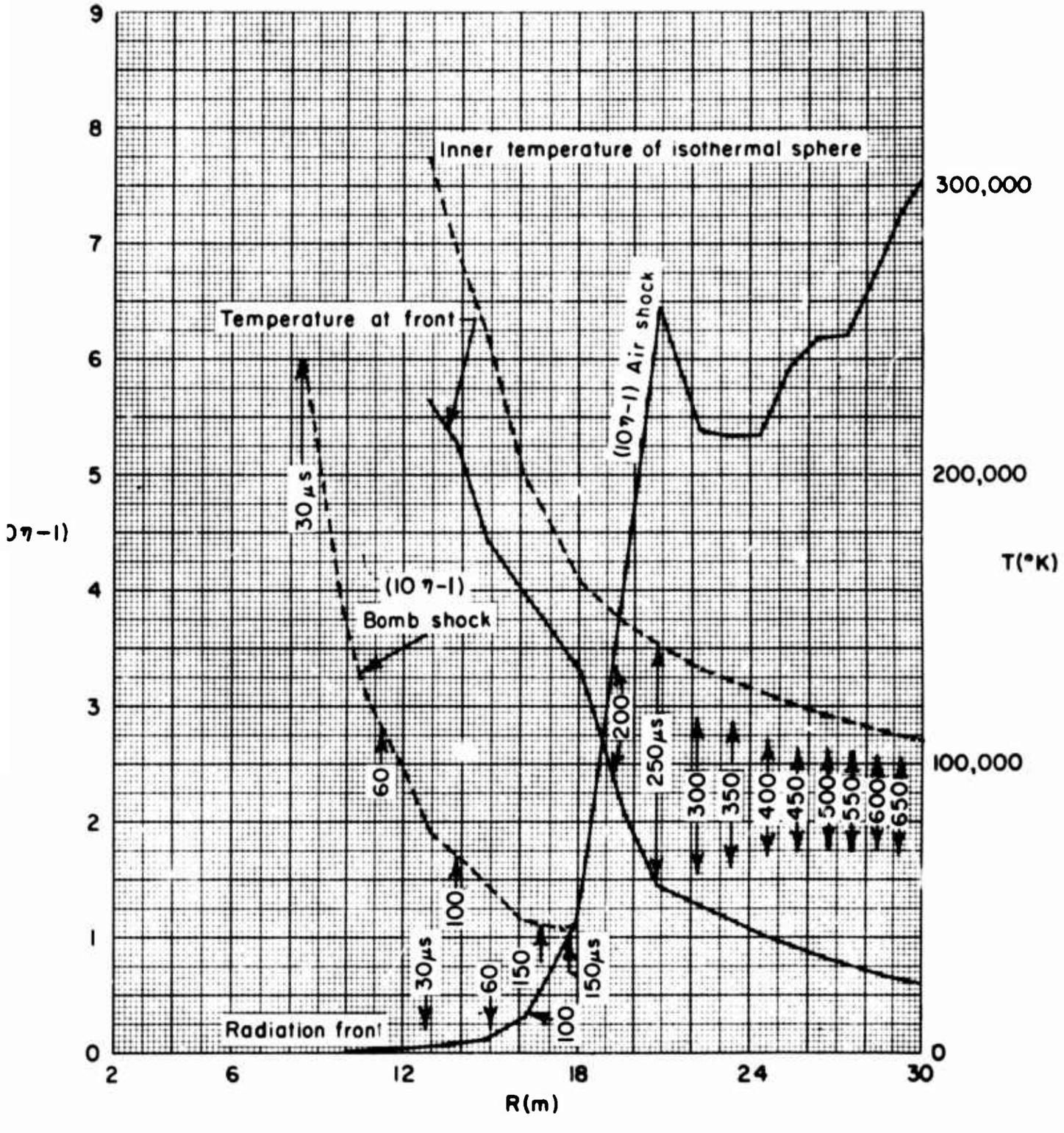

Fig. 52—Radiation diffusion transition to shock $o_i = \rho_0 / 10$

DOCUMENT CONTROL DATA

1. ORIGINATING ACTIVITY THE RAND CORPORATION	2a. REPORT SECURITY CLASSIFICATION UNCLASSIFIED 2b. GROUP

3. REPORT TITLE

NUCLEAR EXPLOSIONS IN CAVITIES

4. AUTHOR(S) (Last name, first name, initial)

Brode, H. L.

5. REPORT DATE	6a. TOTAL NO. OF PAGES	6b. NO. OF REFS.
November 1965	70	12

7. CONTRACT or GRANT NO.	8. ORIGINATOR'S REPORT NO.
AF33(657)-9619	RM-3727

9a. AVAILABILITY/LIMITATION NOTICES	9b. SPONSORING AGENCY
	USAF

10. ABSTRACT

A discussion of underground cavities as an effective means of reducing the seismic signals from nuclear detonations. This Memorandum reports the wall pressures, temperatures, and densities for five specific examples, for which average cavity pressures range between 44 and 420 bars, with peak pressures between 0.2 and 8.2 Kbars. One nuclear yield, 1.7 kilotons, was exploded (theoretically) in two cavities of 20 and 40 meters radius, each with normal and one-tenth normal air density in it. The larger cavity was also used with a density of one-hundredth normal. In addition to the wall pressures, temperatures, and densities as functions of time for each case, some typical pressure, temperature, and density profiles in the cavity interiors at various times are reported.

11. KEY WORDS

Nuclear blasts
Caves
Detection